

**COPPER PHTHALOCYANINES AND FUNCTIONALIZED  
CARBON NANOTUBES**

STUDIES OF ALIGNMENT OF COPPER PHTHALOCYANINE  
COMPOUNDS ON AU(111) AND SIDEWALL  
FUNCTIONALIZATION OF SINGLE-WALLED CARBON  
NANOTUBES WITH SCANNING TUNNELING  
MICROSCOPY

By

GUOXIU WEI, B.Sc., M.Sc.

A Thesis

Submitted to the School of Graduate Studies

in Partial Fulfillment of the Requirements

for the Degree

Master of Science

McMaster University

© Copyright by Guoxiu Wei, August 2005

MASTER OF SCIENCE (2005)

McMaster University

(Chemistry)

Hamilton, Ontario

TITLE: Studies of Alignment of Copper Phthalocyanine Compounds  
on Au(111) and Sidewall Functionalization of Single-  
Walled Carbon Nanotubes with Scanning Tunneling  
Microscopy

AUTHOR: Guoxiu Wei, B.Sc., M.Sc.

SUPERVISOR: Professor Peter Kruse

NUMBER OF PAGES: xiii, 104

## Abstract

This thesis consists of two projects: alignment of copper phthalocyanine compounds on Au(111) and sidewall functionalization of single-walled carbon nanotubes on graphite. Both of these projects are performed with scanning tunneling microscopy (STM), which is used to study the structure of modified surfaces that are of interest in molecular electronics.

In the first project, copper phthalocyanine compounds are made into a thin film with different methods, such as solution deposition, self-assembly and Langmuir-Blodgett film deposition. Those films are important materials in photoelectric devices such as organic light emitting diodes (OLED's). Molecules in these films are aligned on the solid surface with face-on orientation or edge-on orientation. However, the films of molecules with face-on orientation are preferentially used in LED's. In this project, we focus on finding a method to force molecules with face-on orientation in the film. The structure of copper octakisalkylthiophthalocyanine films on Au(111) was investigated with STM under ambient conditions. Columns of molecules are commonly observed due to the  $\pi$ - $\pi$  interaction between molecules. The presence and length of alkyl chains in the molecules affects the alignment of molecules on the gold surface. The weak interaction between molecules and substrate caused the structure to be easily modified by an STM

tip.

In addition, chemical sidewall functionalization of SWCNTs was also explored with STM under ambient conditions. It was found that the spatial distribution of functional groups on nanotube sidewall is not random. Understanding the rules behind the distribution of functional groups will allow scientists to better control carbon nanotube functionalization and improve the properties of nanotubes. High resolution STM images provide direct evidence of the distribution and the effects of functional groups on nanotubes. Possible mechanisms are proposed to elucidate the process of SWCNT functionalization by free radicals and via the Bingel reaction.

## Acknowledgements

I would like to give many appreciations to my supervisor, Dr. Peter Kruse for his help and patience during my two-year study in Canada. He is one of the best professors who I have met since I came here. His kindness made an impression on me. He gave me a lot of help and guidance to resolve the problems which I met during my study. I also want to thank Dr. Alex. D. Bain for his useful suggestions and comments on my research work and my thesis. In addition, Dr. Kalai Saravanamuttu also paid more patience with my thesis and gave many helpful suggestions on my thesis.

Many thanks gave all of my labmates, especially my current labmates Mark Greiner, Hany Ramadan, Sung-Kyun Lee, Kevin Moonosawmy, Arne Kloke, Danish Rizwan, Tom Snyder. They are all very nice. It is easy to get along well with them.

I also want to thank Dr. Holger Eichhorn and his group at University of Windsor for providing chemicals.

In addition, I really appreciate the staffs in the main office, especially Ms. Carol Dada who gave me many encouragements on my English and on my study.

Finally, many thanks gave my parents and my friends. They always encourage me to do what I should do even though I got very bad grades on my studies.

## TABLE OF CONTENTS

	Page
<u>ABSTRACT</u> .....	iii
<u>ACKNOWLEDGEMENTS</u> .....	v
<u>TABLE OF CONTENTS</u> .....	vi
<u>LIST OF SCHEMES</u> .....	x
<u>LIST OF FIGURES</u> .....	xi
<b>Chapter 1: INTRODUCTION</b> .....	1
1.1 Background of scanning tunneling microscopy.....	1
1.2 Design of the projects.....	2
1.2.1 Alignment of copper phthalocyanines (CuPcs) and their derivatives on the Au(111) surface.....	2
1.2.2 Sidewall functionalization of single-walled carbon nanotubes (SWCNTs)	3
References.....	5
<b>Chapter 2: INSTRUMENT AND SAMPLE PREPARATION</b> .....	7
2.1 Introduction of instrument.....	7
2.1.1 Tunneling theory.....	7
2.1.1.1 One dimensional tunneling junction.....	7
2.1.1.2 Common formula to estimate tunneling current.....	9
2.1.2 Working Modes of STM.....	10
2.1.3 Construction of STM.....	11
2.1.4 Artifacts in STM images.....	13

2.1.4.1 Multiple-tip effect.....	13
2.1.4.2 Grain boundary and grain walls on the graphite surface.....	15
2.2 Experimental section.....	18
2.2.1 Tip preparation.....	18
2.2.2 Substrate preparation.....	19
2.2.2.1 The Au(111) surface.....	19
2.2.2.2 The graphite surface.....	21
2.2.3 Organic film preparation.....	22
2.2.3.1 Solution deposition.....	22
2.2.3.2 Self-assembled monolayer (SAM) .....	23
2.2.3.3 The Langmuir-Blodgett films.....	23
References.....	24

## Chapter 3: ALIGNMENT OF COPPER PHTHALOCYANINES

(CuPcs) ON AU(111).....	26
3.1 Introduction of CuPcs.....	26
3.2 Design of the project .....	28
3.3 Structure of CuPc and their derivatives.....	30
3.4 Experimental section.....	31
3.5 Results and Discussion.....	33
3.5.1 Films formed by self-assembly.....	34
3.5.2 The structures of molecules on Au(111) through solution deposition..	40
3.5.3 The Langmuir-Blodgett films of CuPcSC <sub>5</sub> .....	41
3. 5.4 The process of the structure change.....	44

3.5.5 The growth of island.....	45
3.5.6 The diffusion of gold steps in presence of molecules.....	48
3.5.7 The co-adsorption with other molecules.....	50
3.5.8 The structure of the molecules after annealing the sample.....	54
3.6 Conclusions.....	55
References.....	57

## Chapter 4: INTRODUCTION TO SINGLE-WALLED CARBON NANOTUBES (SWCNTs) AND SIDEWALL

FUNCTIONALIZATION.....	60
4.1 History of carbon nanotubes (CNTs).....	60
4.2 Structure of CNTs.....	62
4.3 Studies of SWCNTs with STM and STS in the references.....	65
4.4 Functionalization of SWCNTs.....	67
4.5 Introduction of my project.....	69
References.....	71

## Chapter 5: SIDEWALL FUNCTIONALIZATION OF SINGLE- WALLED CARBON NANOTUBES.....

74	74
5.1 Introduction.....	74
5.2 Experimental section.....	74
5.3 Results and Discussion.....	76
5.3.1 Correlation between the nanotubes within the same bundle.....	76

5.3.2 Periodicity of functional groups.....	85
5.3.3 Change of electronic structure of SWCNTs after functionalization....	90
5.3.4 Mixture of electronic structures in the bundles.....	95
5.4 Conclusions....	99
References.....	99
<b>Chapter 6: CONCLUSIONS.....</b>	<b>102</b>
6.1 Alignment of copper phthalocyanine (CuPc) compounds on Au(111) .....	102
6.2 Sidewall functionalization of SWCNTs.....	103

## List of Schemes

	Page
Scheme 3-1 The optimized structures of a. CuPc b. CuPcSC <sub>5</sub> and c. CuPcSC <sub>8</sub> ..	31
Scheme 4-1 Functionalization of SWCNTs by free radicals.....	70
Scheme 4-2 Functionalization of SWCNTs via the Bingel reaction.....	71

## List of Figures

	Page
Figure 2-1 One-dimensional tunneling junction.....	7
Figure 2-2 The working modes of STM: (a) constant current mode (b) constant height mode.....	11
Figure 2-3 Picture of the ambient STM Digital Instruments Nanoscope II.....	12
Figure 2-4 Illustrations of the process to produce an artifact by a double tip...	13
Figure 2-5 Artifact produced by the multiple tips.....	14
Figure 2-6 Grain boundary on graphite.....	16
Figure 2-7 Grain walls on graphite .....	17
Figure 2-8 STM image of the clean gold surface.....	20
Figure 2-9 Lattice structure of graphite in the reference.....	21
Figure 2-10 STM image of graphite surface.....	22
Figure 2-11 The process to grow a SAM.....	23
Figure 2-12 The process to grow a LB film.....	24
Figure 3-1 Process to form columns of CuPc molecules with face-on orientation.....	29
Figure 3-2 STM image of CuPc on Au(111) .....	35
Figure 3-3 STM image of CuPcSC <sub>5</sub> on Au(111) .....	36
Figure 3-4 STM image of CuPcSC <sub>5</sub> on Au(111) .....	38
Figure 3-5 STM image of CuPcSC <sub>8</sub> on Au(111) .....	40
Figure 3-6 STM image of the deposited CuPcSC <sub>5</sub> molecules on Au(111) .....	41
Figure 3-7 STM images of the Langmuir-Blodgett film of CuPcSC <sub>5</sub> on	

Au(111) .....	42
Figure 3-8 The process of the structure change of molecules.....	44
Figure 3-9 The growth of the island.....	46
Figure 3-10 The sequence of molecular diffusion on the gold steps.....	49
Figure 3-11 The gold surface covered by adsorbates in silver paint.....	50
Figure 3-12 The molecules on the gold surface coated with silver paint.....	52
Figure 3-13 The STM images of the mixture between CuPcSC <sub>5</sub> with stearic acid on Au(111).....	53
Figure 3-14 The annealed sample of CuPcSC <sub>5</sub> .....	54
Figure 3-15 The STM image of the annealed sample of CuPcSC <sub>5</sub> on Au(111)	55
Figure 4-1 TEM images of multi-walled carbon nanotubes	
(a) five graphitic sheet tube, diameter 6.7 nm	
(b) two graphitic sheet tube, diameter 5.5 nm	
(c) seven graphitic sheet tube, diameter 6.5 nm.....	61
Figure 4-2 Electron micrograph of a single-shell carbon nanotube with the diameter about 1.37 nm.....	62
Figure 4-3 Schemes of a SWCNT:	
(a) an extended fullerene molecule with the diameter 0.7 nm	
(b) a graphene tubule by rolling up one single graphene sheet into a cylinder.....	63
Figure 4-4 The construction of a SWCNT from a single graphene sheet.....	64
Figure 4-5 (a, b) STM images of isolated SWCNTs on Au(111). (c, d) Calculated normalized conductance, $(V/I)dI/dV$ and measured I-V (inset) recorded on the nanotube in a, b.....	65

Figure 5-1 (a) The bundles of SWCNTs functionalized by isopentyl radicals	
(b) The scheme of the proposed process of the bundle break.....	79
Figure 5-2 (a) The bundles of SWCNTs functionalized by isopentyl radicals	
(b) The scheme of the proposed process of functionalization. ....	80
Figure 5-3 The functionalized SWCNTs via the Bingel reaction.....	84
Figure 5-4 The functionalized SWCNTs by isopentyl radicals.....	86
Figure 5-5 The functionalized SWCNTs by isopentyl radicals.....	89
Figure 5-6 (a,b) The SWCNTs functionalized via the Bingel reaction.	
(c) The scheme of the graphite surface.....	91
Figure 5-7 (a, b) The process to separate nanotubes from the bundle.....	96

## **Chapter 1**

### **Introduction**

#### 1.1 Background of scanning tunneling microscopy

Since Binnig and Rohrer invented scanning tunneling microscopy (STM) in 1981,<sup>1</sup> it has been developed as an important tool in surface science to investigate the nanostructure on metal or on semiconductor surfaces. It provides a three-dimensional profile of the surface, which is useful for the characterization of surface roughness, observation of phenomena at the interface and determination of the size of nanostructures on the surface. Compared with conventional techniques to study surfaces such as x-ray diffraction and low energy electron diffraction (LEED), STM can investigate various structures not just periodic structures. It gives local information of the surface rather than average information such as infrared spectroscopy (IR). STM images with atomic resolution provide the possibility to study how the molecules adsorb on the surface and to modify the nanostructures.

In my thesis, STM was used as an important analytical instrument to explore the orientations of copper phthalocyanines (CuPcs) and their derivatives on the Au(111) surface. In addition, sidewall functionalization of single-walled carbon nanotubes (SWCNTs) was also investigated with STM on graphite.

## 1.2 Design of the projects

### 1.2.1. Alignment of CuPcs and their derivatives on the Au(111) surface

Many applications for copper phthalocyanines (CuPcs) and their derivatives have been found in organic light emitting diodes (OLEDs), photovoltaic cells or organic electronics. Most of their applications are realized through preparation of CuPcs and their derivatives as thin films. At the electrode surface, the molecules can orient either face-on or edge-on. Due to the strong  $\pi$ - $\pi$  stacking interactions between the molecules, they prefer to form columns with edge-on orientation. However, for applications requiring current transport across the film (e.g. OLEDs), face-on orientation is preferable, because conduction predominantly occurs along the stacked columns.

The goal of my project is to find a molecular system that forces molecular alignment with face-on orientation using molecules that were provided by Prof. Eichhorn's group at the University of Windsor. The molecules containing eight thio-ether groups were expected to form a face-on orientation monolayer at the Au(111) surface, which can function as template during film formation. Such orientation of CuPcs in the film has been reported through the vacuum-deposition method. However, wet-chemical fabrication would be more economical and simple.

In this project, the CuPc films are prepared by wet-chemical fabrication such as

self-assembly, drop-let deposition and the Langmuir-Blodgett technique. The structure of copper octakisalkylthiophthalocyanine films on Au(111) was observed with STM under ambient conditions. Comparing the structures of the organic films formed by the different CuPc derivatives, we found that the length of the alkyl chain in the derivatives affects the orientation of the molecules. In addition, the method of the organic film formation also has an influence on the orientation of the molecules.

### 1.2.2 Sidewall functionalization of single-walled carbon nanotubes

Since their discovery in 1993, single-walled carbon nanotubes (SWCNTs) have attracted a lot of interest due to their unique properties.<sup>2-4</sup> Most of the early work was performed to study their physical properties. More recently, their chemical properties have also drawn much attention. Chemical functionalization is used to improve the solubility of SWCNTs and combine their unique properties with those of other types of materials.<sup>5</sup> Several approaches have been developed to functionalize SWCNTs, such as defect functionalization,<sup>6,7</sup> covalent functionalization of the sidewall, noncovalent functionalization of CNTs wrapped with a conjugated polymer.<sup>8</sup> Among them, chemically covalent functionalization is especially important due to the change of electronic structure of SWCNTs resulting from the attachment of functional groups to the

nanotube. After functionalization, one or two  $sp^2$ -hybridized carbon atoms of SWCNTs are converted into  $sp^3$ -hybridized carbon, which might cause the electronic properties of SWCNTs to change from metallic to semiconducting. Although several analytical techniques such as TEM, SEM and AFM have been used to observe the topography of the functionalized SWCNTs, no information about the distribution and the orientation of functional groups is available through these techniques. The application of STM provides the possibility to investigate the functionalized SWCNTs at a nanometer scale. From STM images of functionalized SWCNTs, the change of electronic structure of SWCNTs can be observed and information about functional groups obtained.<sup>9</sup>

In this project, we investigate the SWCNTs functionalized by free radicals and via the Bingel reaction with STM under ambient conditions. We focus on investigating the spatial distribution of functional groups on the nanotube sidewall, which will be helpful to interpret the effects of functional groups on the electronic structure and mechanical properties of carbon nanotubes. The STM images can provide direct information to explore the mechanism of chemical functionalization of nanotubes, which will be helpful in controlling functional groups on nanotubes. The studies of functionalization of nanotubes will extend the potential applications of nanotubes in nanoelectronic devices.

In this thesis, the electronic structure of SWCNTs after functionalization is

analyzed carefully using atomic resolution images. Possible mechanisms are proposed to elucidate the process of functionalizing SWCNTs by free radicals and via the Bingel reaction. The unique properties of functionalized SWCNTs are observed on graphite.

## References

1. Binnig G, Rohrer H. Scanning tunneling microscopy - from birth to adolescence. Nobel lecture. Dec. 8; 1986.
2. Odom TW, Huang JL, Kim P, Lieber CM. Atomic structure and electronic properties of single-walled carbon nanotubes. *Nature* 1998;391:62-64.
3. Reich S, Thomsen C, Ordejon P. Electronic band structure of isolated and bundled carbon nanotubes. *Phys. Rev. B* 2002;65:155411.
4. Martel R, Schmidt T, Shea HR, Hertel T, Avouris P. Single- and multi-wall carbon nanotube field-effect transistors. *Appl. Phys. Lett.* 1998;73:2447-2449.
5. Hirsch A. Functionalization of single-walled carbon nanotubes. *Angew. Chem. Int. Ed.* 2002;41:1853-1859.
6. Chen J, Hamon MA, Hu H, Chen Y, Rao AM, Eklund PC, Haddon RC. Solution properties of single-walled carbon nanotubes. *Science* 1998;282:95-98.
7. Hamon MA, Chen J, Hu H, Chen YS, Itkis ME, Rao AM, Eklund PC, Haddon

- RC. Dissolution of single-walled carbon nanotubes. *Adv. Mater.* 1999;11:834-840.
8. Star A, Stoddart JF, Steuerman D, Diehl M, Boukai A, Wong EW, Yang X, Chung SW, Choi H, Heath JR. Preparation and properties of polymer-wrapped single-walled carbon nanotubes. *Angew. Chem. Int. Ed.* 2001;40:1721-1725.
9. Kelly KF, Chiang IW, Mickelson ET, Hauge RH, Margrave JL, Wang X, Scuseria GE, Radloff C, Halas NJ. Insight into the mechanism of sidewall functionalization of single-walled nanotubes: an STM study. *Chem. Phys. Lett.* 1999;313:445-450.

## Chapter 2

### Instrument and sample preparation

#### 2.1 Introduction of instrument

Scanning tunneling microscopy (STM) plays an important role in the development of surface science. Its resolution can reach a few angstroms in lateral direction and less than one angstrom in vertical direction.<sup>6</sup> It can give a topographical image of surface structure. In my thesis, STM is a main instrument to investigate the structure of copper phthalocyanines (CuPcs) on the gold surface and the sidewall functionalization of single-walled carbon nanotubes (SWCNTs) on gold or on graphite. In order to understand the reason that this instrument was chosen to perform my projects, it is necessary to know the principle of electron tunneling and the construction and working modes of STM.

##### 2.1.1 Tunneling theory

###### 2.1.1.1. One dimensional tunneling junction

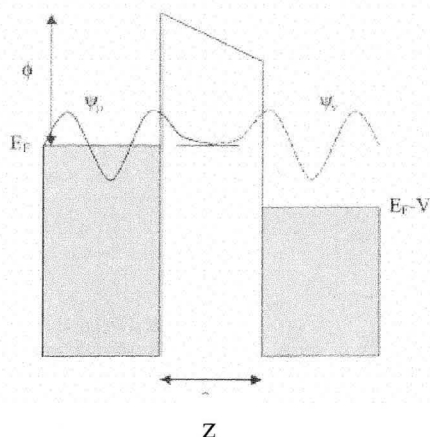


Figure 2-1 One-dimensional tunneling junction.<sup>3</sup>  $z$  is the distance between the tip and the sample.

STM is built on the basis of electron tunneling, which is not allowed in classical mechanics but in quantum mechanics.<sup>7</sup> As shown in Figure 2-1, an electron with energy ( $E$ ) at Fermi level can pass through a barrier  $\phi > E$  according to quantum mechanics. In STM, due to the overlap of wave functions between tip and sample, electrons can pass through the vacuum barrier from the tip to the sample (or from the sample to the tip) when a bias voltage is applied to the sample.

According to quantum mechanics, a small number of electrons can traverse the barrier between the tip and the sample if the distance  $z$  between the tip and the sample is very small. In the classically forbidden region, the wave function  $\psi$  can be expressed by the following equation:<sup>3,7</sup>

$$\psi(z) = \psi(0) \exp\left[-\frac{\sqrt{2m(\phi - E)}}{\hbar} z\right] \quad (2.1)$$

In the equation,  $m$  is the mass of the electron,  $\hbar$  is Planck's constant /  $2\pi$ ,  $z$  is the distance between the tip and the sample,  $E$  is the energy of the electron, and  $\phi$  is the potential barrier height. From the equation, it can be seen that the wave function  $\psi$  decreases exponentially with the distance  $z$ .

In STM, the tunneling current  $I_t$  is related to the probability that an electron passes through the barrier. Through considering the density of states of the sample  $\rho_s(E_F)$  at the Fermi level into the Equation 2.1, the tunneling current  $I_t$  can be predicted by the

following formula:<sup>3,7</sup>

$$I_t \propto V \rho_s(E_F) \exp \left[ -2 \frac{\sqrt{2m(\Phi - E)}z}{\hbar} \right] \quad (2.2)$$

In the above formula,  $\Phi$  is the barrier potential in eV,  $z$  is the distance between the tip and the sample in angstrom units and  $\rho_s(E_F)$  is the density of states of the sample of the Fermi level. From the formula, it can be seen that the tunneling current decays exponentially with the distance  $z$  between the tip and the sample.

The model of a one-dimensional tunneling junction explains the process to produce tunneling current. However, STM works on a three-dimensional geometry, which indicates that a new model will be used to interpret the tunneling phenomena in STM.

#### 2.1.1.2 Common formula to estimate tunneling current

In the experiment, the sharp metal tip, which is usually made of Pt/Ir or W, is approaching the flat sample surface until the distance between the tip and the sample is small enough to produce a tunneling current. The tunneling current can be simply predicted by the following equation.<sup>3,7</sup>

$$I = C \rho_t \rho_s e^{-z * k^{1/2}} \quad (2.3)$$

Here,  $z$  is the sample-tip separation,  $\rho_t$  is the tip electronic structure,  $\rho_s$  is the sample

electronic structure, and  $C$  is a constant. The tunneling current  $I$  is exponentially dependent on the sample-tip separation  $z$ .  $k$  is equal to  $\frac{\sqrt{2mE}}{\hbar}$ .

### 2.1.2 Working Modes of STM

STM can image the sample surface in two working modes: constant current mode and constant height mode.

In constant current mode, the tunneling current is kept constant under the control of a feedback loop while a bias voltage is applied to the sample (or the tip). According to the equation (2.3), a constant tunneling current leads to a constant distance between the tip and the sample. When the tip is scanned over the sample surface, the vertical position of the tip is changed to maintain the constant distance as shown in Figure 2-2a. The motion of the tip in three directions ( $x$ ,  $y$  and  $z$ ) is controlled by piezoelectric elements on the STM scanner. When voltage ramps are applied to the scanner, the tip begins to scan over the surface. In the constant current mode, the STM image is recorded as a 3-dimensional image, which usually represents the surface topography. However, sometimes the STM image is not consistent with the surface topography because it is related to contours of constant local density of states (LDOS) at the Fermi level.

In an alternative working mode, constant height mode, the feedback loop is turned

off when the tip begins to scan the surface. The tip height remains constant during the imaging process as shown in Figure 2-2b. When the tip scans over the surface, the surface topography causes the distance between the tip and the sample to change, which results in the change of tunneling current. This mode is applied to scan the surface at a high speed. However, it is required that the surface must be very smooth to avoid crashing the tip.

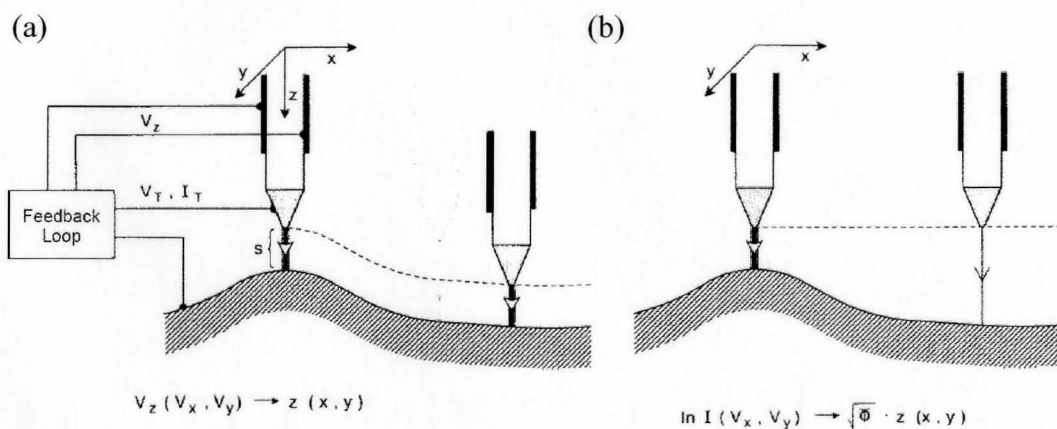


Figure 2-2 The working modes of STM: (a) constant current mode (b) constant height mode.<sup>2</sup>

### 2.1.3 Construction of STM

All STMs are composed of five parts: the metal tip, the scanner, the detector, the electronic control system (computer) and the vibration isolation system. In my projects, the ambient STM Digital Instruments Nanoscope II is used to study the adsorption of copper phthalocyanines (CuPcs) and the sidewall functionalization of single-walled

carbon nanotubes SWCNTs. The Digital Instruments Nanoscope II is shown in Figure 2-3.

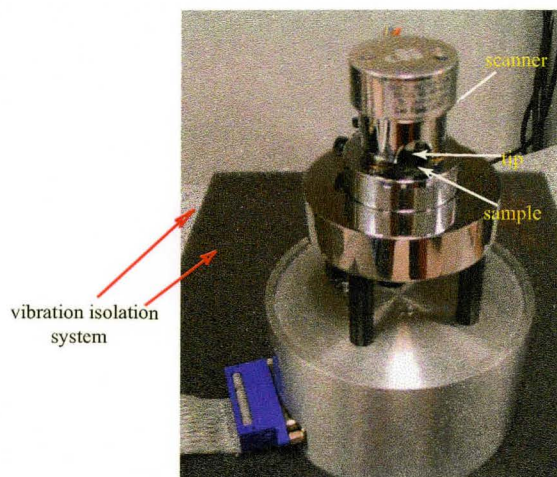


Figure 2-3 Picture of the ambient STM Digital Instruments Nanoscope II

The STM tip is usually made of Pt/Ir or W. It is inserted into the tip hole of the scanner. The distance between the tip and the sample is less than 1 nm under the control of the tip approach system.

In order to obtain a good signal, the STM must have a high mechanical stability. Due to the small tunneling current and the high resolution of STM images with 1.0 Å laterally and 0.1 Å vertically, it is required that noise from any source must be smaller than 0.1 Å in the lateral directions and 0.01 Å in the vertical direction. The vibration isolation systems can effectively decrease the influence of noise on the STM. In our ambient STM, foam material is used to decrease vibration as shown in Fig. 3. In addition,

the STM is also put on a stone column to decrease the vibration from the ground.

#### 2.1.4 Artifacts in STM images

In the experiments with STM, various artifacts are observed due to factors such as the tip geometry, local variations in properties and local topography of surface. Here, we give some examples of the artifacts produced by the STM tip or by the topography of the sample surface.

##### 2.1.4.1. Multiple-tip effect

The tip's microscopic structure has a large influence on the imaging performance of the tip. The process to produce an artifact by a double tip is illustrated in Figure 2-4. The different distance between the minitips and the surface caused the false heights of adsorbate.

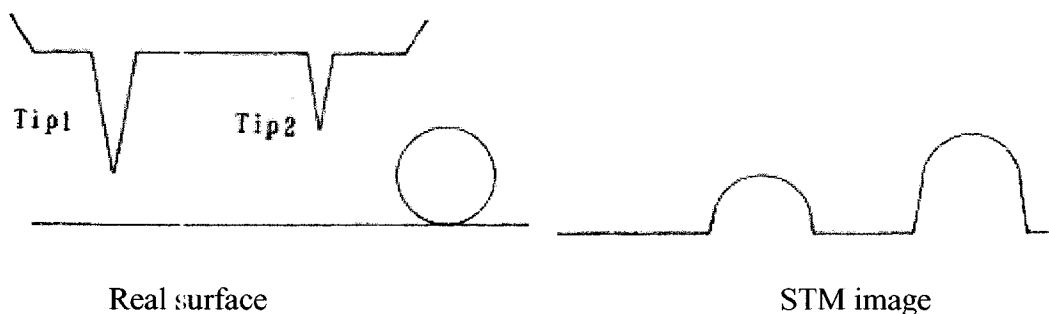


Figure 2-4 Illustrations of the process to produce an artifact by a double tip.<sup>5</sup>

During the observation of the functionalized SWCNTs on the graphite surface, the STM image produced by the multiple tips was obtained as shown in Figure 2-5. Except for a few lines which may be nanotubes or the steps of graphite, four graphene sheets with a characteristic shape appear on the graphite surface as circled by the dashed rings in Figure 2-5. Those graphene sheets have almost the same shape and are parallel to each other. These features indicate that the multiple tips caused the reproduced graphene sheets in Figure 2-5. If this STM image is not analyzed carefully, it can lead to misrepresentations of the alignment of the functionalized SWCNTs on graphite and the wrong conclusions about the functionalized SWCNTs.



Figure 2-5 Artifact produced by the multiple tips.

Scan size: 300 nm × 300 nm

#### 2.1.4.2 Grain boundary and grain walls on the graphite surface

Graphite is commonly used as a substrate due to the ease of preparing clean and flat surfaces and easy imaging. In the recent years, carbon nanotubes (CNTs) were deposited on graphite and investigated with STM. The interaction between the nanotube and the graphite surface similar to the interaction between layers of the graphite sheets assists anchoring of the nanotube on the graphite surface.<sup>8</sup> However, the presence of grain boundary and grain walls on graphite causes difficulties in determining the structure of nanotubes. They might be mistaken as functionalized CNTs on graphite. Therefore, it is very important to distinguish artifacts and nanotubes during our study.

Figure 2-6 shows the STM image of a grain boundary on the graphite surface. The grain boundary appears as a band with some kinks. It is made up of many peaks

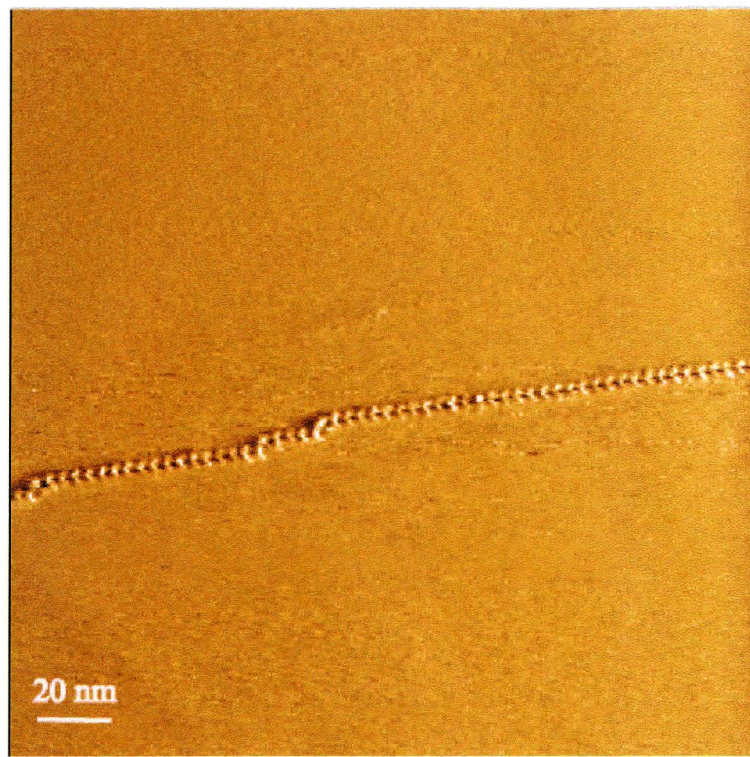


Figure 2-6 Grain boundary on HOPG. scan size:  $200 \text{ nm} \times 200 \text{ nm}$ .  
 $V_B = 700 \text{ mV}$ .  $I_T = 1 \text{ nA}$ . Scan rate:  $2.48 \text{ Hz}$

with a characteristic shape. The peaks are aligned with a periodicity about  $3.6 \text{ nm}$ . The shape of this grain boundary is very similar to the “peak-valley” appearance of grain boundary with about  $5 \text{ nm}$  distance between neighboring peaks as reported by Gan and his coworkers.<sup>9</sup> The periodic peaks are easily mistaken for functional groups on CNTs. However, when increasing the scan rate to a high value, a grain boundary can not be moved around. At high scan rates, nanotubes tend to be moved by the STM tip, as reported in the reference.<sup>10</sup>

During our observation on the graphite surface, another artifact was shown in Figure 2-7. The structure exhibited in Figure 2-7 appears as two twisted nanotubes, which is very similar to the structure of domain walls reported by Binnig and his coworker.<sup>11</sup> Domain walls were previously mistaken for DNA strands.<sup>12</sup> They are formed by the misfit of two crystal orientations of graphite layers. Binnig<sup>11</sup> reported an effective way to distinguish grain walls and grain boundaries. If the structure was a grain boundary or a grain wall, the angle between the lattice directions on both sides of boundary would not be  $60^\circ$  or  $120^\circ$ . This method is used to determine the structure exhibited in Figure 2-7.

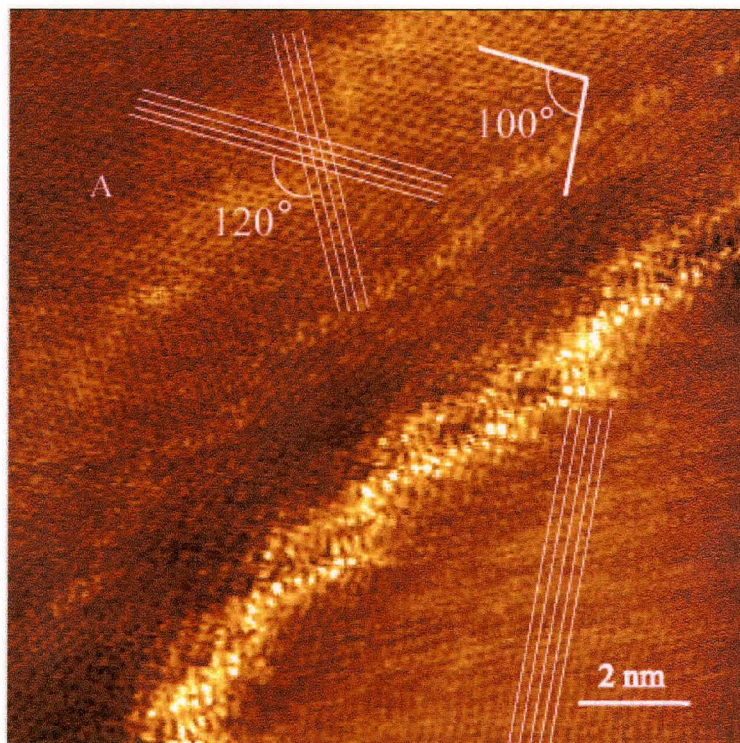


Figure 2-7 Grain walls on HOPG. Scan size:  $13.5 \text{ nm} \times 13.5 \text{ nm}$ .  $V_B = 100 \text{ mV}$ .  $I_T = 1 \text{ nA}$ . Scan rate:  $19.53 \text{ Hz}$

The lattice structures on both sides of grain walls are determined with a little thermal drift, which is attributed to the STM imaging mechanism of the highly curved nanostructures resulting in the image atomic lattice being stretched.<sup>13</sup> The thin parallel lines in Figure 2-7 are drawn along the directions of the graphite lattice. In the area A without grain walls, the angle between two lattice directions of the graphite substrate is about 120°. However, the angle between the lattice directions on both sides of grain walls is about 100° as shown by the thick lines in Figure 2-7. Therefore, the structure in Figure 2-7 was determined to be a grain wall on graphite.

In addition to the artifacts mentioned above, Simonis and his coworkers found a new artifact, the double helix superstructure on graphite.<sup>14</sup> The existence of various artifacts on graphite is a reminder that the structure observed on graphite must be analyzed carefully.

## 2.2 Experimental section

### 2.2.1 Tip preparation

There are two methods to fabricate the STM tip. They are mechanical forming and electrochemical etching. The material of the tip is usually the Pt-Ir wire or the tungsten wire.

In the thesis, the mechanical method is mainly used to make the STM tip. Through cutting the end of the 0.25 mm Pt-Ir wire with scissors, a sharp tip is formed. Then it is washed with Millipore water. After this, the Pt-Ir tip is ready to be used in STM.

Another method prepare a tip is through electrochemical etching. The material of the tip is often tungsten wires. In this method, a tungsten wire with 0.25 mm diameter was immersed into the electrolyte as working electrode. The electrolyte can be a 1-5 M KOH or NaOH solution and the counter electrode can be a Pt wire. The immersed part of the tungsten wire is etched when the current is passed between the electrodes. The etching process occurs preferentially at the meniscus of the solution and a neck at the surface is formed along the tungsten wire. With time, the immersed part of the tungsten wire falls off into solution. The etching process stops at the same time. The produced tip is washed with Millipore water. This method can be also used to make an Au or Pt-Ir tip with different electrolyte.

## 2.2.2 Substrate preparation

### 2.2.2.1 The Au(111) surface

In my projects, the Au(111) surface was obtain through annealing the gold films

(150-200 nm thick) deposited on a glass slide. They were purchased from Arrande Company. Due to the lowest energy of Au(111) among the gold crystal surfaces such as Au(111), Au(110) and Au(100), it is preferentially formed after annealing the gold film.

Before start to anneal it, the gold film was put into 98% sulfuric acid for half a day to remove organic contamination. Then the gold film was washed with Millipore water. After cleaning it, the gold film was annealed in a butane flame three times. Then it cooled to room temperature in air.

After that, the gold surface was observed with STM. One of the clean gold surface images is shown in Figure 2-8. Atomic-scale steps appear on the surface. The angle between the steps is about  $60^\circ$  or  $120^\circ$  as shown by the arrows in Fig. 8. This feature indicates that the surface is the Au(111) surface. It is consistent with the lowest energy of the Au(111) surface.



Figure 2-8 STM image of the clean gold surface.  
Scan size: 200nm × 200nm

### 2.2.2.2 The graphite surface

Graphite is another substrate in my project. It is also called highly oriented pyrolytic graphite (HOPG). The clean surface is prepared through cleaving one layer of graphite with tape. This works because graphite is a layered material as illustrated in Figure 2-9.

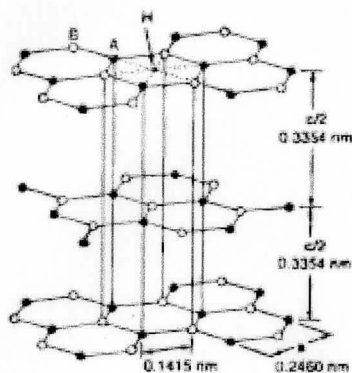


Figure 2-9 Lattice structure of graphite in reference.<sup>4</sup>

One STM image of the graphite surface is obtained as shown in Figure 2-10. The carbon atoms of graphite are oriented along three directions as shown by the black arrows in Figure 2-10. The angle between three directions is  $60^\circ$  or  $120^\circ$ . The distance between neighboring protrusions is about  $0.24 \text{ nm}$ . These results are consistent with the calculated result by Toussaint's group.<sup>4</sup>

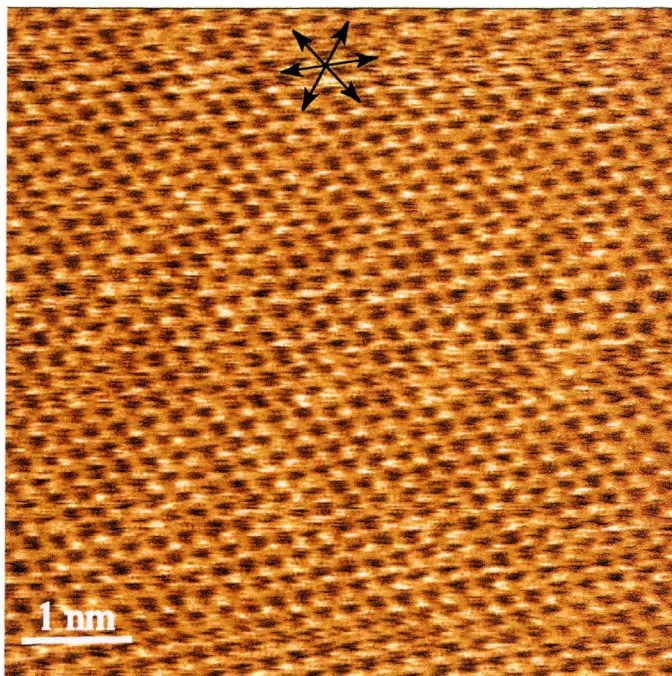


Figure 2-10 STM image of graphite surface

### 2.2.3 Organic film preparation

During investigating the alignment of molecules on a solid surface, several methods are used to prepare organic films of molecules. In my thesis, three different methods are applied. They are solution deposition, self-assembly and the Langmuir-Blodgett technique. Each method is introduced in the following paragraphs.

#### 2.2.3.1 Solution deposition

One method to form organic film on the solid surface is solution deposition. The investigated chemicals are dissolved into organic solvent. Then one droplet of solution is

added on the substrate. After evaporation of the organic solvent, the molecules are left on the substrate. Due to the interaction between the molecules or between the molecule and the substrate, the molecules may form a certain pattern.

This method is also used to deposit carbon nanotubes on graphite.

### 2.2.3.2 Self-assembled monolayer (SAM)<sup>1</sup>

In this method, the prepared substrate is put into the solution containing the molecules. Due to the interaction between the molecules and the substrate atoms, a pattern will be formed without human invention. The process to grow a SAM is illustrated in Figure 2-11.

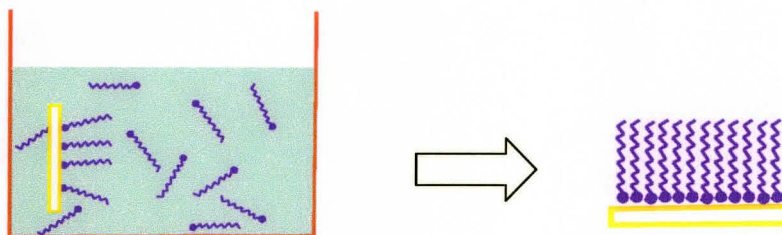


Figure 2-11 the process to grow a SAM

### 2.2.3.3 The Langmuir-Blodgett films<sup>1</sup>

With the help of a former summer student Sherdeep Singh, copper phthalocyanines are prepared as Langmuir-Blodgett (L-B) films. The process to form a L-B film is shown in Figure 2-12. First, copper phthalocyanines with alkyl chains are deposited on a water surface with a syringe. Due to hydrophilic-hydrophobic interaction,

molecules will spread on the water surface. The resultant film is called a Langmuir film. Then, the Langmuir film is transferred on a solid substrate. The film on the solid substrate is called a Langmuir-Blodgett film. By repeating the dipping process, multilayers can be prepared.

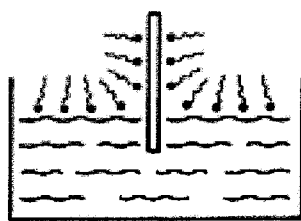


Figure 2-12 The process to grow a L-B film<sup>1</sup>

In the next chapters, the applications of these methods will be explained and exhibited in detail. The experiment results will be discussed.

## References

1. Schreiber F. Structure and growth of self-assembling monolayers. *Prog. Surf. Sci.* 2000;65:151-256.
2. Binnig G, Rohrer H. Scanning tunneling microscopy - from birth to adolescence. Nobel lecture. Dec. 8; 1986.
3. Meyer E, Hug HJ, Bennewitz R. Scanning probe microscopy: The Lab on a tip. Berlin, Germany: Springer-Verlag; 2004. 15-23 p.

4. Toussaint U, Schimmel T, Kupperts J. Computer simulation of the AFM/LFM imaging process: hexagonal versus honeycomb structure on graphite. *Surf. Interface Anal.* 1997;25:620-625.
5. Hu J, Gu M, Wang Z, Yao X, Xu Y, Zhang L, Huang Z, Zhu J, Li M. Multiple-tip effect on scanning tunneling microscope images of deoxyribonucleic acid. *Jpn. J. Appl. Phys.* 1992;31:110-113.
6. Leemput LEC, Kempen H. Scanning tunneling microscopy. *Rep. Prog. Phys.* 1992;55:1165-1240.
7. Bonnell DA. Scanning probe microscopy and spectroscopy: theory, techniques, and applications. New York, USA: A John Wiley & Sons. Inc.; 2001. 7-42 p.
8. Rettig C, Bodecker M, Hovel H. Carbon-nanotubes on graphite: alignment of lattice structure. *J. Phys. D: Appl. Phys.* 2003;36:818-822.
9. Gan Y, Chu W, Qiao L. STM investigation on interaction between superstructure and grain boundary in graphite. *Surf. Sci.* 2003;539:120-128.
10. Worsley KA, Moonosawmy KR, Kruse P. Long-range periodicity in carbon nanotube sidewall functionalization. *Nano Lett.* 2004;4:1541-1546.
11. Heckl WM, Binnig G. Domain walls on graphite mimic DNA. *Ultramicroscopy* 1992;42-44:1073-1078.
12. Clemmer CR, Beebe TP. Graphite - a mimic for DNA other biomolecules in scanning tunneling microscope studies. *Science* 1991;251:640-642.
13. Ge M, Sattler K. Scanning tunneling microscopy of single-shell nanotubes of carbon. *Appl. Phys. Lett.* 1994;65:2284-2286.
14. Simonis P, Goffaux C, Thiry PA, Biro LP, Lambin P, Meunier V. STM study of a grain boundary in graphite. *Surf. Sci.* 2002;511:319-322.

## Chapter 3

### Alignment of copper phthalocyanines on Au(111)

#### 3.1 Introduction of copper phthalocyanines

Since copper phthalocyanines (CuPcs) were discovered during the synthesis of *o*-cyanobenzamide in 1907, they have been used as dyes, pigments and catalysts in industry.<sup>1,2</sup> More recently, they attract interest in gas sensor,<sup>3</sup> molecular optoelectronic<sup>4</sup> and electronic devices<sup>5</sup> due to their semiconducting properties. Compared with other molecules, phthalocyanine compounds demonstrate one of their advantages that they have strong adsorption in the visible and near infrared region.<sup>6</sup> However, the realization of their applications depend on the formation of high-quality CuPc films. The structure and orientation of molecules in the thin film have an influence on the properties of electronic devices. Therefore, it is important to obtain the information about organization and orientation of molecules in the films.

Scanning tunneling microscopy (STM) is found to be an effective tool to investigate the structure of CuPc films on the solid surface. As early as in 1989, Mizutani and his coworkers found that CuPc molecules were arranged into a striped pattern in the

films on graphite through STM.<sup>7</sup> On the basis of STM combined with X-ray diffraction (XRD), Wang and his coworkers found that CuPc molecules on graphite formed the regular close-packed structure in the horizontal direction and face-to-face stacked into columns, whose axis is perpendicular to the graphite surface.<sup>8</sup> On the Au(111) surface, Chizhov and his coworkers investigated the influence of steps on the arrangement of CuPc molecules in the monolayer films.<sup>9</sup> Compared with two different phthalocyanine compounds, Lu and his coworkers found that CoPc molecules probably have a stronger ability to be adsorbed on Au(111) than CuPc molecules in ultrahigh vacuum.<sup>10</sup> Except the above studies of CuPc, its derivatives with alkyl chains form a regular pattern lying flat on graphite.<sup>11</sup> However, the octasubstituted phthalocyanine molecules formed cofacial rodlike aggregates with edge-on orientation in the Langmuir-Blodgett films on Au(111).<sup>12</sup> Those previous studies indicate that the CuPc molecules and their derivatives can form face-on orientation and edge-on orientation, which depend on the properties of molecules and the methods to prepare thin films. This is consistent with the observation of Boden and his coworkers that the headgroups in the molecule will affect the orientation of the molecules in a organic thin film formed by the different methods.<sup>13</sup>

In addition, phthalocyanine compounds are mixed with porphyrin or alkane derivatives to form a thin film.<sup>14-16</sup> It was found that the presence of other molecules

assists phthalocyanine molecules to arrange into a regular pattern. The interaction between two different molecules is proposed to be van der Waals force.

Those previous studies provide very useful information to design our project. On the basis of those studies, we chose the Au(111) surface as a substrate, the CuPc compounds with eight alkyl chains as main objects and the wetting chemical methods to prepare a thin film. We expected that through simple methods, CuPc molecules with alkyl chains could form a regular pattern with face-on orientation in the thin films.

### 3.2 Design of the project

CuPc films, especially their derivative films, have potential applications in electronic devices, such as organic light emitting diodes (OLEDs), photovoltaic cells or organic electronics.<sup>17,18</sup> At the electrode surface, the molecules can orient either face-on or edge-on, with edge-on being the normally preferred orientation because of very strong  $\pi$ - $\pi$  stacking interactions between the molecules. For applications requiring current transport across the film (e.g. OLEDs), however, face-on orientation is preferable, because conduction predominantly occurs along the  $\pi$ -stacked columns.<sup>19</sup>

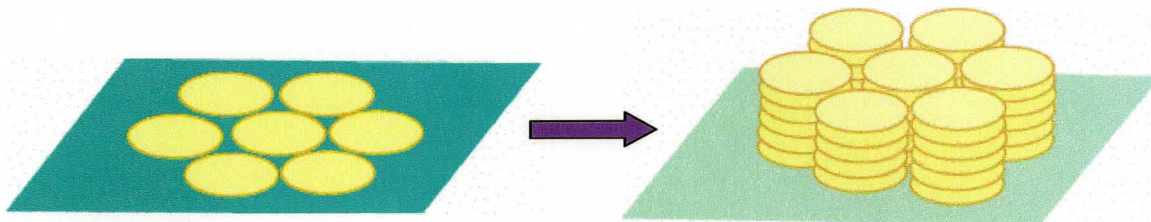


Figure 3-1 Process to form columns of CuPc molecules with face-on orientation

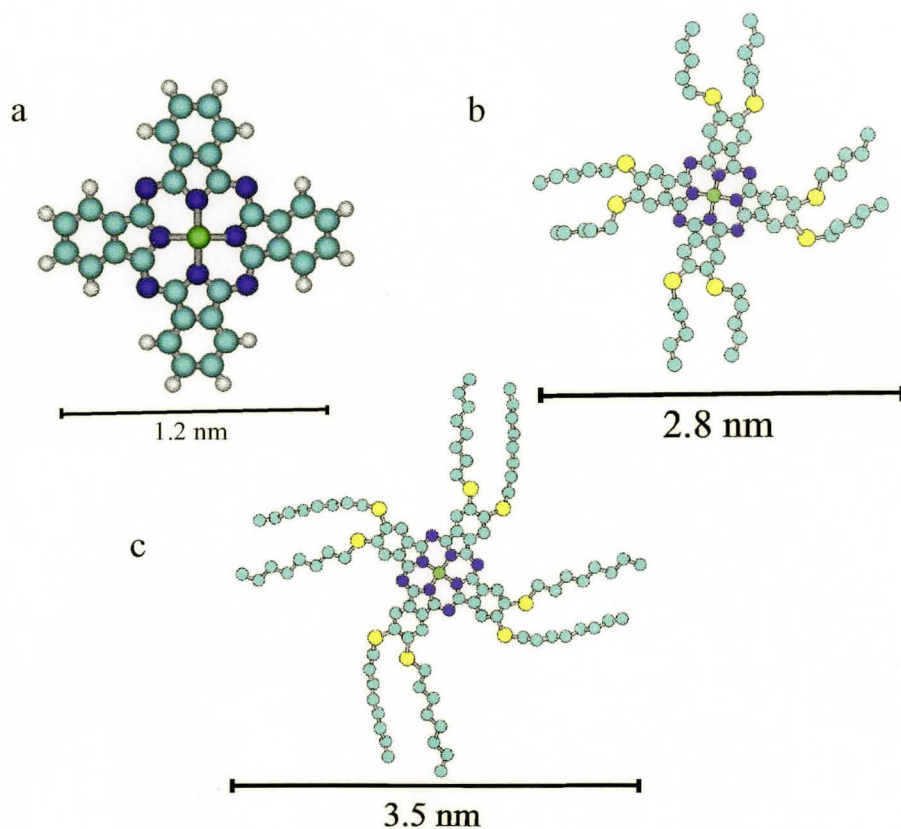
In order to obtain the direct information of CuPc molecules on the electrode surface, the Au(111) surface was used as a substrate. In this project, the purpose focused on finding a molecular system that forces molecules to align at the electrode surface with face-on orientation. Then the adlayer functions as template during the film formation as shown in Figure 3-1. Although the molecules with face-on orientation have been observed in vacuum,<sup>8</sup> the cost of preparation of thin films is much higher than that in wet-chemical fabrication. Using the ambient STM, the films of CuPc molecules with eight thio-ether groups were investigated on Au(111). Solution deposition, self-assembly and the Langmuir-Blodgett technique are used to prepare thin films of CuPc compounds. Through comparing arrangement and orientation of molecules in the films produced by different methods, we will choose the best route to make molecules form face-on orientation.

### 3.3 Structure of copper phthalocyanine and their derivatives

In this project, the molecules to be investigated are copper phthalocyanine (CuPc) and their derivatives with eight thio-ether groups. We expected that the introduction of sulfur atoms into molecule would increase the interaction between molecules and the gold surface due to the formation of the sulfur-gold bond.

The structures of the molecules are as shown in Scheme 3-1. They are optimized by HyperChem 6.0 version. The sizes of CuPc, CuPcSC<sub>5</sub> and CuPcSC<sub>8</sub> are about 1.2 nm, 2.7 nm and 3.5 nm, respectively, which are very useful during the analysis of STM images.

These molecules of CuPcSC<sub>5</sub> and CuPcSC<sub>8</sub> are provided by Prof. Eichhorn's group at University of Windsor. They introduced a new approach to synthesize CuPcSC<sub>5</sub> and CuPcSC<sub>8</sub> molecules as reported in the reference.<sup>6,20</sup>



Scheme 3-1 The optimized structures of a. CuPc b. CuPcSC<sub>5</sub> and c. CuPcSC<sub>8</sub>. In the structures, green dots stand for copper, blue dots are nitrogen atoms, cyan dots are carbon atoms, yellow dots are sulfur atoms and white dots are hydrogen atoms.

### 3.4 Experimental section

CuPc (sublimation grade) was purchased from Sigma-Aldrich (St. Louis, USA). The CuPcSC<sub>5</sub> and CuPcSC<sub>8</sub> molecules were provided by Prof. Eichhorn's group at University of Windsor. Toluene (99.9%, HPLC) was purchased from Sigma-Aldrich (St. Louis, USA). The gold films (150-200 nm thick) deposited on the glass slides (12 mm ×

12 mm) were purchased from Arrandee (Werther, Germany).

Before annealing the gold film, it was put into 95-98% sulfuric acid for half a day to remove organic contamination. Sulfuric acid (95-98%, reagent) was purchased from Sigma-Aldrich (St. Louis, USA). Then, the gold film was washed by Millipore water. After cleaning the gold film, it was annealed by butane flame three times. Then it was cooled to room temperature in air.

Three methods were used to make the CuPc, CuPcSC<sub>5</sub> and CuPcSC<sub>8</sub> films: self-assembly, solution deposition and the Langmuir-Blodgett techniques. The first method is to put the annealed gold substrate into the solution with the concentration of less than 1  $\mu$ M in toluene for 5 minutes. Then it is washed with pure toluene. The second one is to add one droplet of the solution of the molecules with the concentration of less than 1  $\mu$ M on the gold film. After a few minutes, toluene evaporates in air and the molecules stay on Au(111) to probably form a regular pattern, which depends on the interaction between molecules and the gold surface and the interaction between molecules. Those interactions are mainly van der Waals force.

With the help of a former summer student Sherdeep Singh, these molecules were also prepared as the Langmuir-Blodgett films with the KSV2000 system. Under the control of a computer, one barrier compressed the molecular film along the horizontal

direction. The molecular film was floating on the water. One filter paper (1.2 cm  $\times$  1.2 cm) hanging on the balance was used as the Wilhelmy plate. A homemade trough (75 cm  $\times$  34 cm) was made of polytetrafluoroethylene (PTFE).

CuPcSC<sub>5</sub> and CuPcSC<sub>8</sub> are dissolved into chloroform, respectively. The concentration of the solution is 10 mg/ml. An amount of solution was deposited on the water by a syringe. The two-layer film of CuPcSC<sub>5</sub> and the ten-layer film of CuPcSC<sub>8</sub> are both transferred on the annealed gold surface at surface pressure 15 mN/m with deposition speed of 10 mm/min.

The films prepared by solution deposition, self-assembly or the Langmuir-Blodgett deposition were investigated with the Nanoscope II (Digital Instruments, Santa Barbara, CA) under ambient conditions. The STM tip was mechanically cut Pt/Ir wire (90/10). All the STM images were captured under constant current working mode.

The structures in Scheme 3-1 were optimized with Software HyperChem 6.0 version. The method is molecular mechanics method at the MM+ (bond dipoles) level. The algorithm is Polak-Ribiere (conjugate gradient) in vacuo. The termination is 30 cycles.

### 3.5 Results and Discussion

### 3.5.1 Films formed by self-assembly

Before the CuPc molecules were adsorbed on the gold surface, the annealed surface was not observed by STM in order to prevent contamination. Using the self-assembly method, CuPcs formed one thin layer on the Au(111) surface.

From the STM image as shown in Figure 3-2, we can see many many bright dots randomly distributed. The size of the bright dots circled by the dashed ring is about 2.6 nm, two times larger than the calculated size of an individual CuPc molecule of about 1.2 nm. It indicates that the CuPc molecules might aggregate with each other to form large clusters. The bright dots are not homogeneous. Some of them are much larger than others as shown by one example circled by one large ring. Due to the  $\pi$ - $\pi$  attraction between molecules, CuPc molecules prefer to form cofacial stacks. Compared with the interaction between the molecules within cofacial stacks, the interaction between the edge of molecules and the gold surface is much weaker leading to the irregular structure of the films. However, the complexity of the CuPc molecule system prevents us from obtaining quantitative information from calculation. In addition, we found that CuPcs without alkyl chain are very difficult to dissolve in toluene. From their poor solubility, we can suggest that even though a small amount of the molecules are diluted in the solution, they tend to form stacks due to the strong  $\pi$ - $\pi$  interaction between molecules. This might be one

reason that the CuPc molecules formed an irregular pattern on Au(111). The introduction of alkyl chain into the CuPc molecules can increase their solubility in organic solvent, at the same time it can increase the contact area between the molecules and the substrate potentially leading to the formation of a regular pattern.

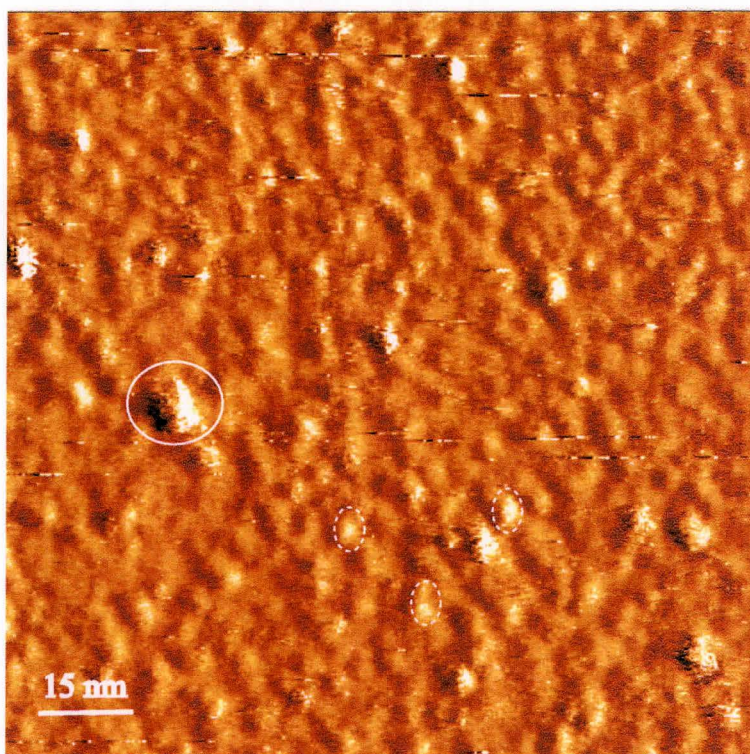


Figure 3-2 STM image of CuPc on Au(111). scan size: 117.4 nm  $\times$  117.4 nm.  $V_B = 700$  mV.  $I_T = 0.5$  nA. Scan rate: 19.53 Hz

A similar method is used to prepare the CuPcSC<sub>5</sub> monolayer on the Au(111) substrate. The STM image of the CuPcSC<sub>5</sub> monolayer is shown in Figure 3-3. The molecules form the regular bands with about 3.7 nm width, larger than the calculated size of the molecule of 2.7 nm. This area with a regular pattern is more than 100 nm × 100 nm. We think that the molecules are aligned with an edge-on orientation on the gold surface. However, it is very difficult to obtain high-resolution images where individual molecules are resolved in the bands, probably due to the thermal movement of alkyl chains.

An STM image is formed by 400 lines of 400 pixels. The typical scan speed in air is 8.48 Hz, which means 8.48 lines/s. The STM captures one image in about 47 s, which is much slower than the frequency of the molecular thermal movement. This is the reason that we can not observe the individual molecules at that time.

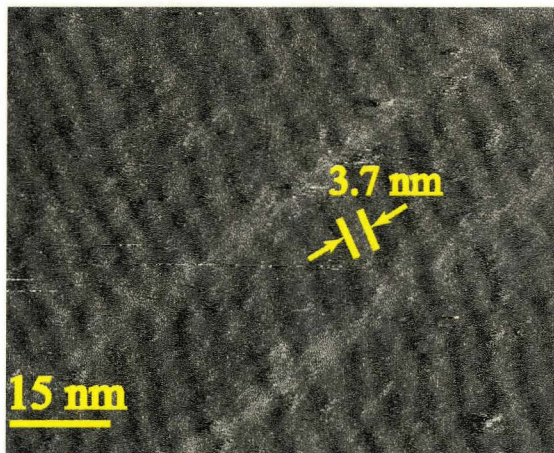


Figure 3-3 STM image of CuPcSC<sub>5</sub> on Au(111). scan size: 81.7 nm × 81.7 nm.  
 $V_B = 800$  mV.  $I_T = 0.8$  nA. Scan rate: 19.53 Hz

In Figure 3-3, we can see the contrast in the stripes cross the columns of molecules. The bright stripes can be attributed to the molecules adsorbed on the gold steps or in the area of surface defects.

Through repeating the same experiment, molecules are observed to arrange themselves into rows on the gold surface. In the area **A** circled by the white dashed elliptical ring in Figure 3-4, a few bright dots are aligned in a line, which size is about 1.6 nm smaller than the calculated size of a CuPcSC<sub>5</sub> molecule of about 2.8 nm, which indicates that all the alkyl chains in the molecules are not imaged. Each bright dot stands for one molecule. In the area **B** circled by the blue dashed elliptical ring, two rows of molecules formed one band, which means that the band can be composed of one or two rows of molecules. It indicates that the molecules interact with the gold surface through weak van der Waals force. The sulfur atom in the thio-ether groups can not form a strong chemical bond to the gold surface. The weak interaction between molecules and the gold surface leads to the irregular patterns.

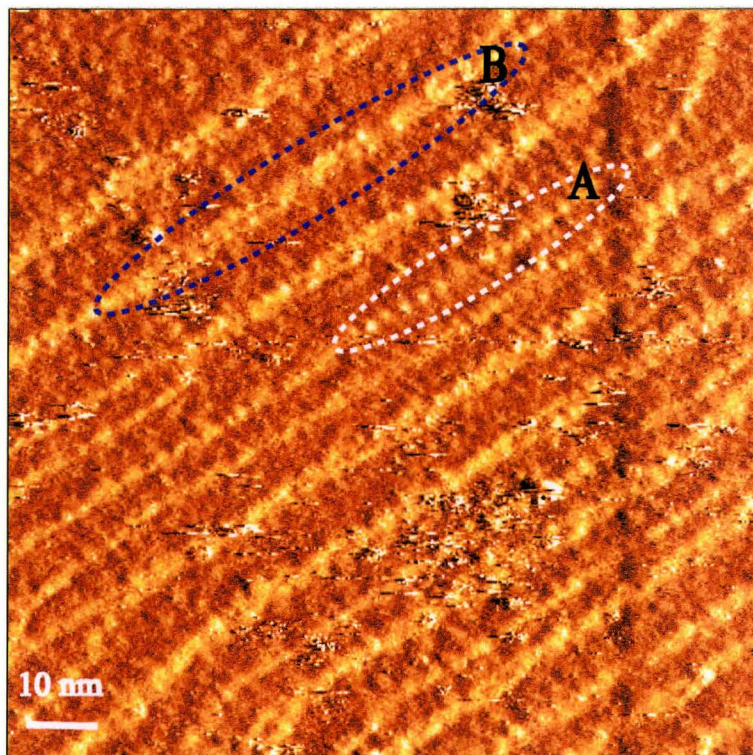


Figure 3-4 STM image of CuPcSC<sub>5</sub> on Au(111). Scan size: 103 nm × 103 nm.  
 $V_B = 1100$  mV.  $I_T = 0.2$  nA. Scan rate: 5.79 Hz

Although we did the same experiments, we observed the different organization of molecules. It indicates that the condition of the gold surface will affect the structure of molecules on the gold surface because we can not obtain the exactly same gold surface each time. Sometimes more defects exist on the gold surface. Sometimes the surface is very rough. Such factors have an influence on the structure of molecules on the gold

surface.

When we used the molecules with the longer alkyl chains, we obtained the STM image as shown in Figure 3-5. In the small area, we can see the bands are not uniform. Through measuring the width of the bands, the smallest band is about 3.0 nm. Compared with the calculated size of the CuPcSC<sub>8</sub> molecule and their cores, the width of the bands was smaller than the size of the molecule and larger than the size of their cores. It means that the cores of the molecules are laid down on Au(111). However, the substituted alkyl chains are not stretch completely. They might be interdigitated with the alkyl chains of the neighboring molecule or become curved. The band with 3 nm in width should be the single molecular row. Through carefully observing the band, it can be seen that the band is composed of small spots in a line. No high-resolution image was obtained which can be attributed to the movement of the molecules and the alkyl chains, consistent with previous observation. In addition, the broader band is about 6 or 9 nm in width. It means that the molecules aggregate to some extent. Two or three rows of the molecules formed one band. However, every molecular row was separated in one band with difficulty. It might be the reason that the interdigitated alkyl chains covered the cores of the neighboring molecules. We also found the disordered structure in the image. We think

that CuPcSC<sub>8</sub> have two orientations on the gold surface. In a word, CuPcSC<sub>8</sub> molecules are not stable on Au(111) and some of them aggregated with each other.

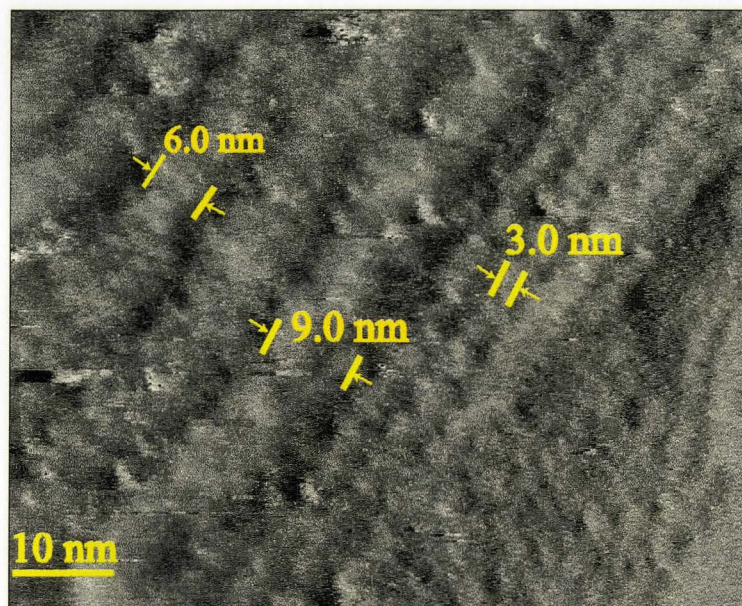


Figure 3-5 STM image of CuPcSC<sub>8</sub> on Au(111). Scan size: 72 nm × 72 nm.

$V_B = 800$  mV.  $I_T = 0.4$  nA. Scan rate: 8.68 Hz

### 3.5.2 The structures of molecules on Au(111) through solution deposition

One simple method is also used to prepare a thin film on the gold surface. One droplet of the solution above was added on the gold surface. After the evaporation of organic solvent, the molecules are left and form a pattern through the interaction between molecules and between the molecules and the substrate.

The STM image in Figure 3-6 is shown the structure of CuPcSC<sub>5</sub> film with this method. The molecules tend to form the bands with different width. It indicates that this kind of molecules prefer to form an irregular pattern and aggregate together due to the  $\pi$ - $\pi$  interaction between molecules. The interaction between molecules and the gold surface is too weak to form a regular structure. In addition, no individual molecules can be observed as shown in Figure 3-6.

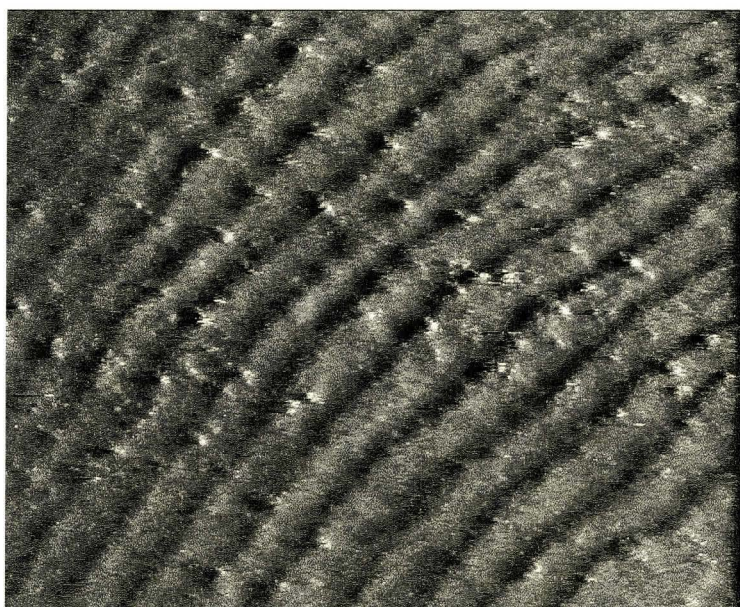


Figure 3-6 STM image of the deposited CuPcSC<sub>5</sub> molecules on Au(111).  
Scan size: 200 nm  $\times$  200 nm.  $V_B = 800$  mV.  $I_T = 1$  nA. Scan  
rate: 8.68 Hz.

### 3.5.3 The Langmuir-Blodgett films of CuPcSC<sub>5</sub>

Through using KSV2000 system, the 2-layer Langmuir-Blodgett film of CuPcSC<sub>5</sub>

was deposited on the annealed gold film at surface pressure 15 mn/m with a deposition speed of 10 mm/min. This work was done by a former summer student Sherdeep Singh. After the Langmuir-Blodgett was prepared, the sample was checked by STM within 1h. It was found that the top layer of the molecules was removed with scanning.

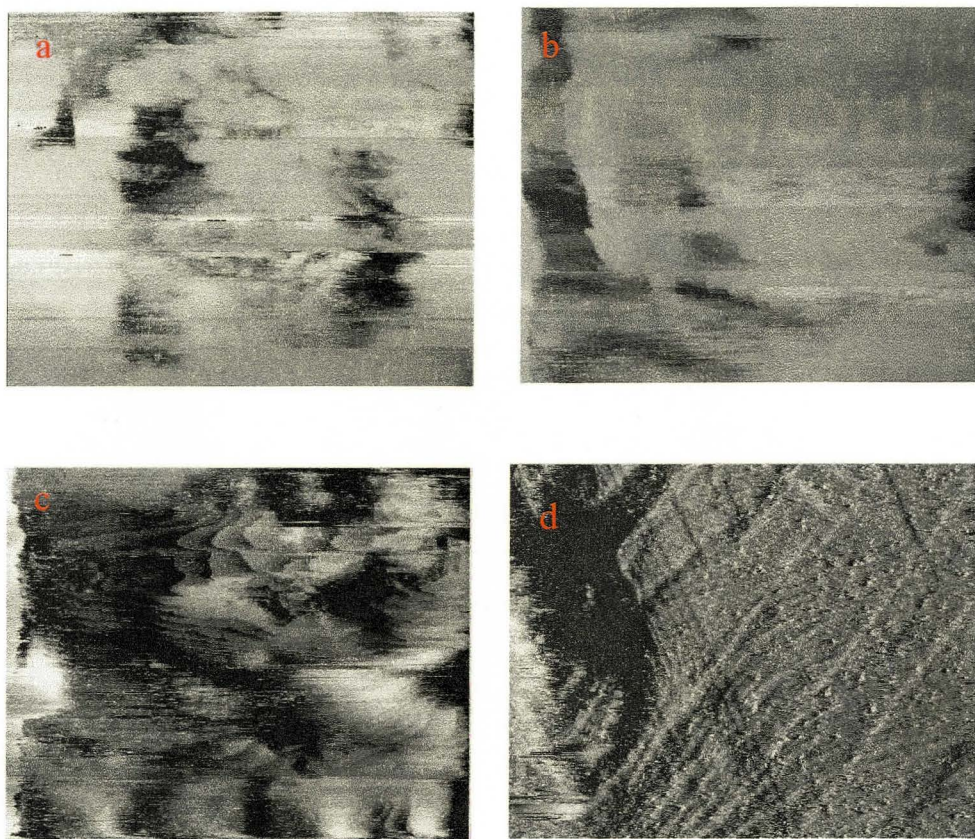


Figure 3-7 STM images of the Langmuir-Blodgett film of  $\text{CuPcSC}_5$  on  $\text{Au}(111)$ .  
Scan size:  $200 \text{ nm} \times 200 \text{ nm}$ .  $V_B = 800 \text{ mV}$ .  $I_T = 1 \text{ nA}$ . Scan rate:  
 $4.34 \text{ Hz}$ .

As shown in Figure 3-7, it was observed that the topmost layer was removed with

tip scanning over the surface and the lower layer with bands appeared. It suggested that the interaction between the layer and the layer was very weak compared with the interaction between the lower layer and the substrate. The alkyl chains made the molecules more easily glide on the surface than the Pc without substituted alkyl chains. Therefore, the scanning tip had a large influence on the stability of the adsorption of the molecules.

Through the observation of Langmuir-Blodgett films, we did not find that CuPcSC<sub>5</sub> or CuPcSC<sub>8</sub> molecules form a regular pattern. From the isotherm graph of CuPcSC<sub>5</sub> or CuPcSC<sub>8</sub> obtained by Sherdeep Singh, we found that surface pressure 15 mN/m is located in the region where the molecules lie flat on the water surface. It means that in the Langmuir-Blodgett films, molecules have face-on orientation. However, they form an irregular pattern, which can be attributed to the weak interaction between molecules. When molecules float on the water surface, only the interaction between molecules plays a role in the arrangement of molecules. However, this interaction is not strong enough to form a regular pattern. Then, this film with an irregular pattern is transferred on the gold surface.

However, during the formation of the molecule films with the methods self-assembly and solution deposition, the interaction between molecules and the gold surface

can assist molecules to form a regular pattern except the interaction between molecules. It indicates that the formation of the regular structure of molecules depends on the cooperation of all the factors.

### 3. 5.4 The process of the structure change

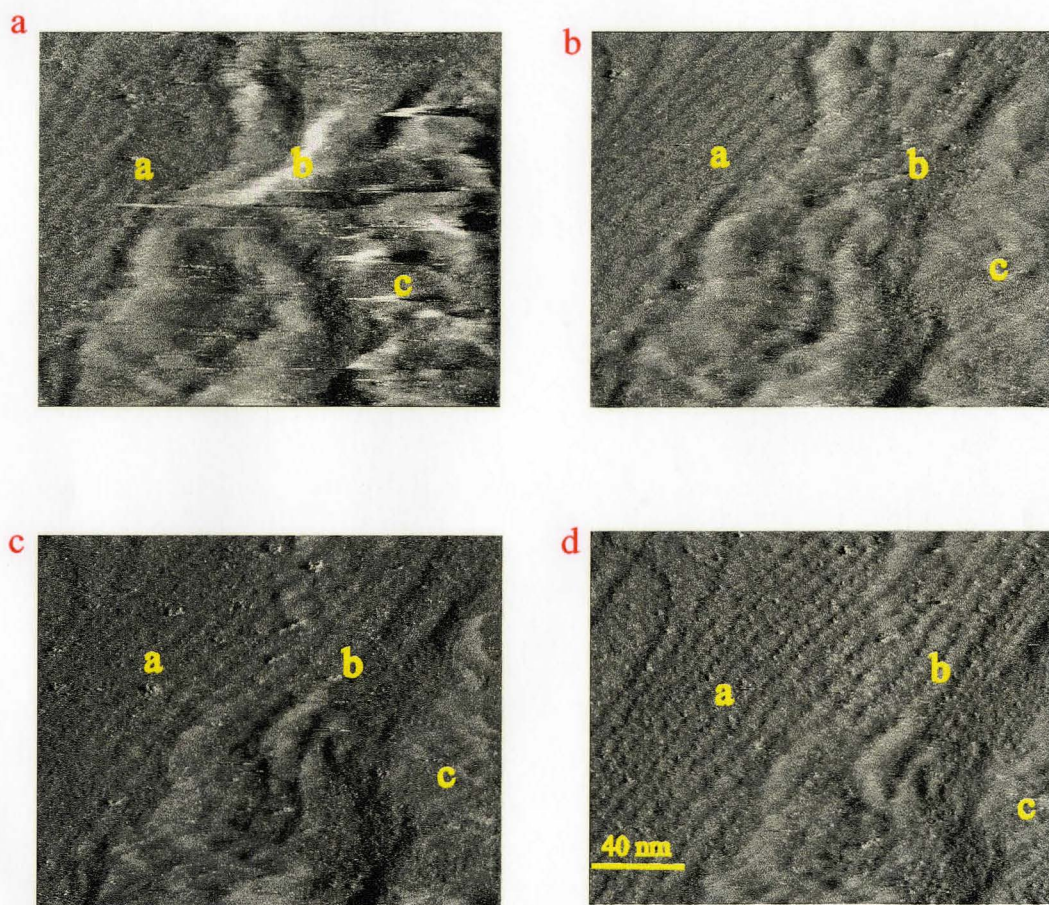


Figure 3-8 The process of the structure change of molecules.

Scan size: 25.7 nm  $\times$  25.7 nm.  $V_B = 407$  mV.  $I_T = 0.8$  nA. Scan rate: 19.53 Hz.

From Figure 3-8a, several straight bands can be seen. In the area **b** and **c**, protruding islands appeared on Au(111). After 95s of continuous scanning, it was obviously seen that the straight bands in area **a** became clear and increased in length as shown in Figure 3-8b. In the area **b**, the protruding island disappeared and the bands tended to be formed. There was also a big change in area **c**. The island became smaller than before and the surface became flat. After 285s, the bands in area **a** of Figure 3-8c became more obscure than those of Figure 3-8b. However, the straight bands became clear in area **b**. In area **c**, the surface continued to become flat and there was no band to appear. Figure 3-8d showed the STM image after 856s. In the area **b**, bands with different width existed. Because of the drift of the image, the area **c** was not observed completely. According to the changes in area **a**, **b**, **c**, it can be concluded that the change should be attributed to the adjustment of the CuPcSC<sub>8</sub> molecules adsorbed on Au(111) with the help of the STM tip. The interaction between molecules and the gold surface is very weak.

### 3.5.5 The growth of island

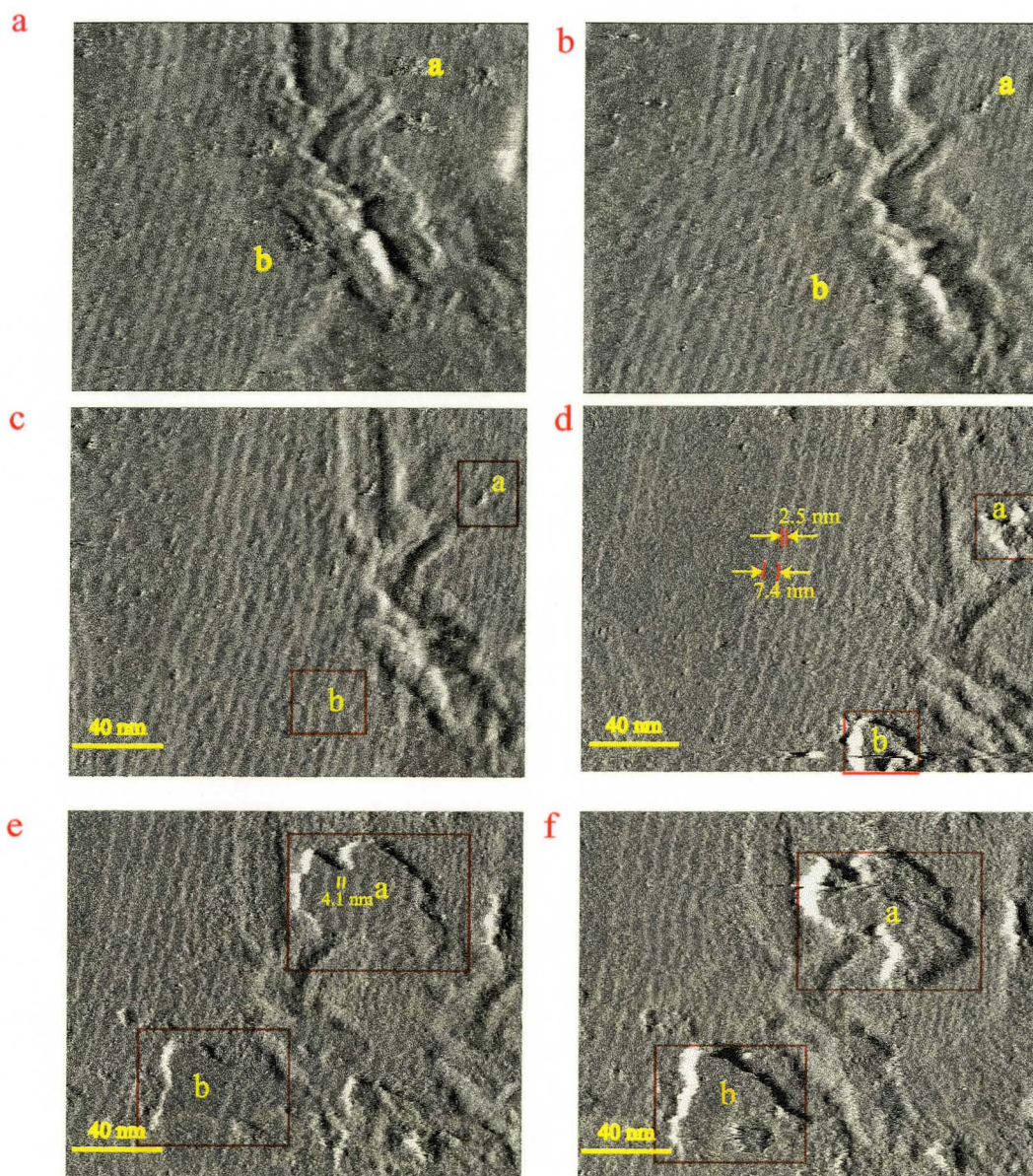


Figure 3-9 The growth of the island. Scan size:  $200 \text{ nm} \times 200 \text{ nm}$ .

$V_B = 800 \text{ mV}$ .  $I_T = 1 \text{ nA}$ . Scan rate:  $4.34 \text{ Hz}$ .

During observing the self-assembled monolayer of CuPcSC<sub>5</sub>, the process to grow an island was reported as shown in Figure 3-9. After start to scan the surface for a few minutes, the ordered bands appeared in the domain **a** as shown in Figure 3-9a. They are straight and have the almost uniform width with about 4.1 nm, which is larger than the calculated 2.8 nm size of the molecule. It is possible that every band is composed of two molecular rows and the alkyl chains are interdigitated with those of the neighboring molecules. The distance between the interbands is about 6.6 nm. The space is enough for every molecule lying on Au(111) with the alkyl chains parallel to the surface. In the area **b** which is next to the gold steps, the molecules formed the disordered structures. They tended to adsorb along the gold steps, consistent with the previous report.<sup>6</sup> Through continuing to observe the surface for more than 50 min in the same place, it was found that the bands are not stable on Au(111) and tended to become disordered. They began to twist. The width of the bands became smaller than before, at about 2.5 nm as shown in Figure 3-9d. This is likely due to the plane of the molecule tilting with respect to the Au(111) surface. In addition, the distance between the neighboring bands became heterogeneous and increased gradually to about 7.4 nm. It might be attributed to the repulsive force from the alkyl chains of CuPcSC<sub>5</sub>. An interesting phenomenon can be observed in Figure 3-9d, e and f. The new adlayer **a** is growing up very fast in the leaf

area from Figure 3-9d to e. The new layer **a** appears to be a new layer on top of the monolayer. It can be also seen that the molecules formed the ordered bands in the area **a**. The width of the bands is about 4.1 nm. It is indicated that the bands might be composed of two rows of the molecules flat on the surface. However, after more than 1 minutes, the height of the area **a** continues to increase. The area **a** becomes rough and finally formed an island. The ordered bands decreased in length and became distorted. At the same time, the area **b** became larger gradually and its height continued to increase. From this phenomenon, we can know that CuPcSC<sub>5</sub> does not easily form monolayer, but has a tendency to form multiplayer. This means that the interaction between the molecules is comparable to the interaction between the molecule and the substrate. Due to mobility of the molecule on Au(111), it is difficult to get high resolution STM images to determine the orientation of CuPcSC<sub>5</sub>.

### 3.5.6 The diffusion of gold steps in presence of molecules

When the molecules are prepared a Langmuir-Blodgett film deposited at surface pressure 15 mN/m with a deposition speed of 10 mm/min, we find a very interesting phenomenon as shown in Figure 3-10. As the tip scanned the surface, the number of the light lines continued to decrease. It has been reported previously that in presence of

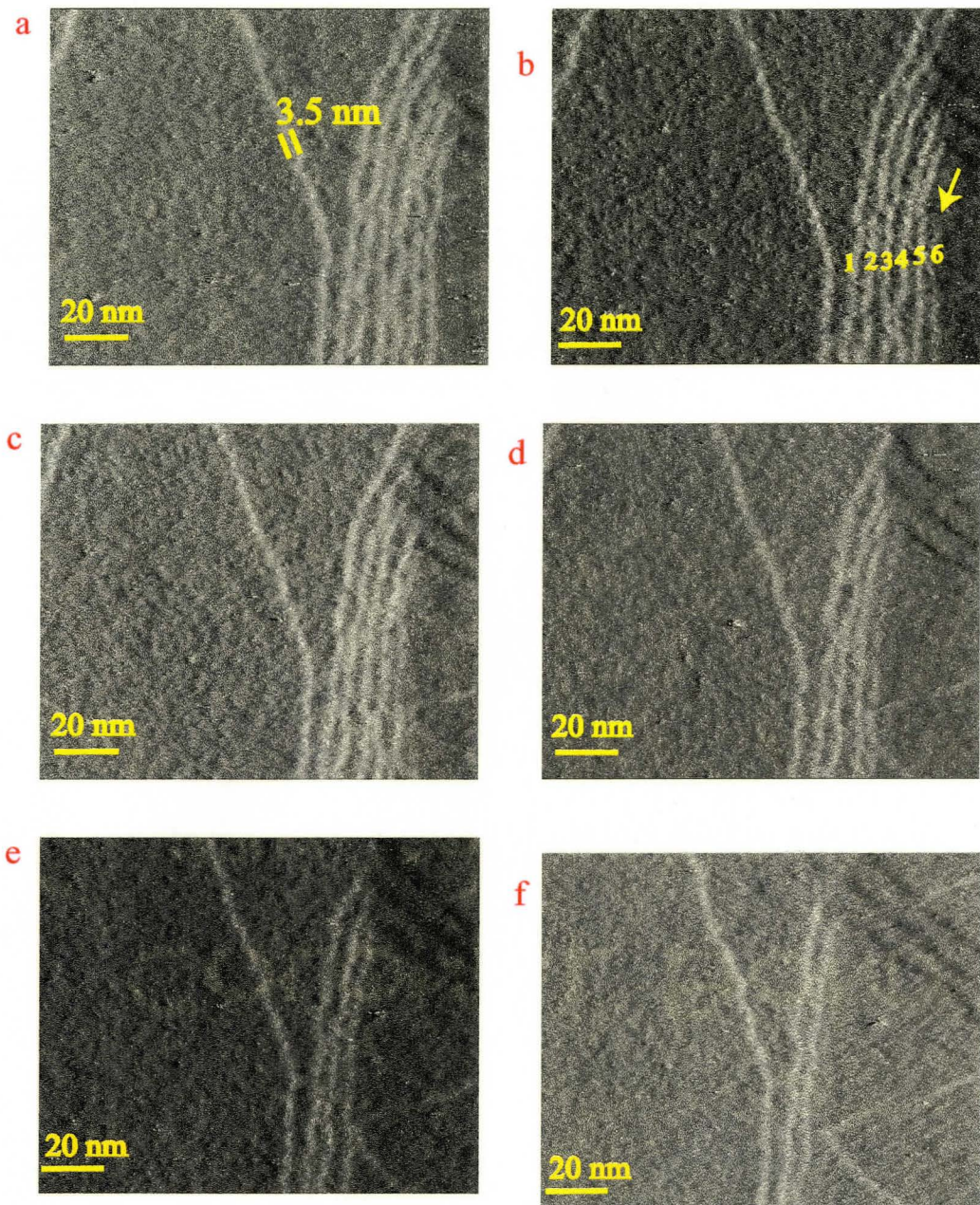


Figure 3-10 The sequence of molecular diffusion on the gold steps. Scan size:  $200 \text{ nm} \times 200 \text{ nm}$ . (a, b, c, d)  $V_B = 800 \text{ mV}$ .  $I_T = 1 \text{ nA}$ . Scan rate:  $4.34 \text{ Hz}$ . e,  $V_B = 410.8 \text{ mV}$ .  $I_T = 1.07 \text{ nA}$ . f,  $V_B = 410.8 \text{ mV}$ .  $I_T = 1.67 \text{ nA}$ .

adsorbate molecules, the diffusion energy of Au atoms decreases. With the help of the tip, molecules on the gold steps or gold atoms in the light lines can diffuse on the surface.

### 3.5.7 The co-adsorption with other molecules

To prepare one sample for STM, we used silver paint to connect a silver wire with the gold substrate. However, the silver paint covered the half of the gold surface. Using STM, adsorbates can be observed on the clean gold surface as shown in Figure 3-11.



Figure 3-11 The gold surface covered by adsorbates in silver paint.  
Scan size: 200 nm  $\times$  200 nm.  $V_B = 800$  mV.  $I_T = 1$  nA.

Alcohol is one of the main ingredients of silver paint. It was possible that alcohol is the main source of the multilayer. After a drop of the CuPcSC<sub>5</sub> solution (about 1  $\mu$ M) was added on the contaminated gold surface, an STM image as shown in Figure 3-12a was obtained. The molecules formed a very regular structure. The size of each bright spot is about 3.5 nm, larger than the size of the molecule. The distance between neighboring molecules is about 7 nm. In addition, every spot appears to include two small spots as shown by two white rings in Figure 3-12a, which are not well separated. We suggest that the molecules formed a dimer. Every spot stands for one cluster. When zooming out as shown in Figure 3-12b, it can be seen that the molecules form two domains **a** and **b**. In the area **a**, the distance between the molecules is homogeneous. However, in the area **b**, the distance between the molecules is different. It can be attributed to the difference of the properties in the different area due to the adsorption of silver paint. They made the property of every part of the gold surface different.

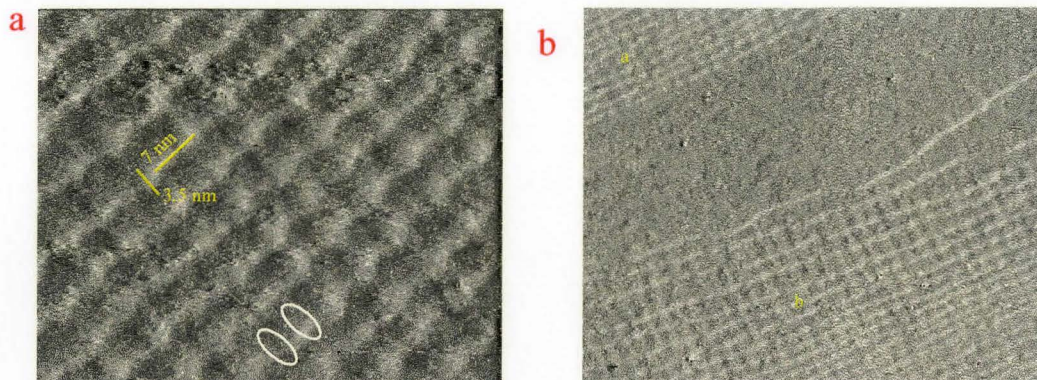


Figure 3-12 The molecules on the gold surface coated with silver paint.

a, Scan size:  $56.6 \text{ nm} \times 56.6 \text{ nm}$ .  $V_B = 800 \text{ mV}$ .  $I_T = 1 \text{ nA}$ .

b, Scan size:  $139.8 \text{ nm} \times 139.8 \text{ nm}$ .  $V_B = 800 \text{ mV}$ .  $I_T = 1 \text{ nA}$ .

In this project, the mixture of  $\text{CuPcSC}_5$  and stearic acid (1:3) was dissolved in toluene. Then the annealed gold substrate was put into the solution to prepare the self-assembled monolayer of the mixture. It was found that the molecules form a regular pattern on the gold surface. A lot of rows of molecules appear as shown in Figure 3-13a. In the STM image with large magnification as shown in Figure 3-13b,

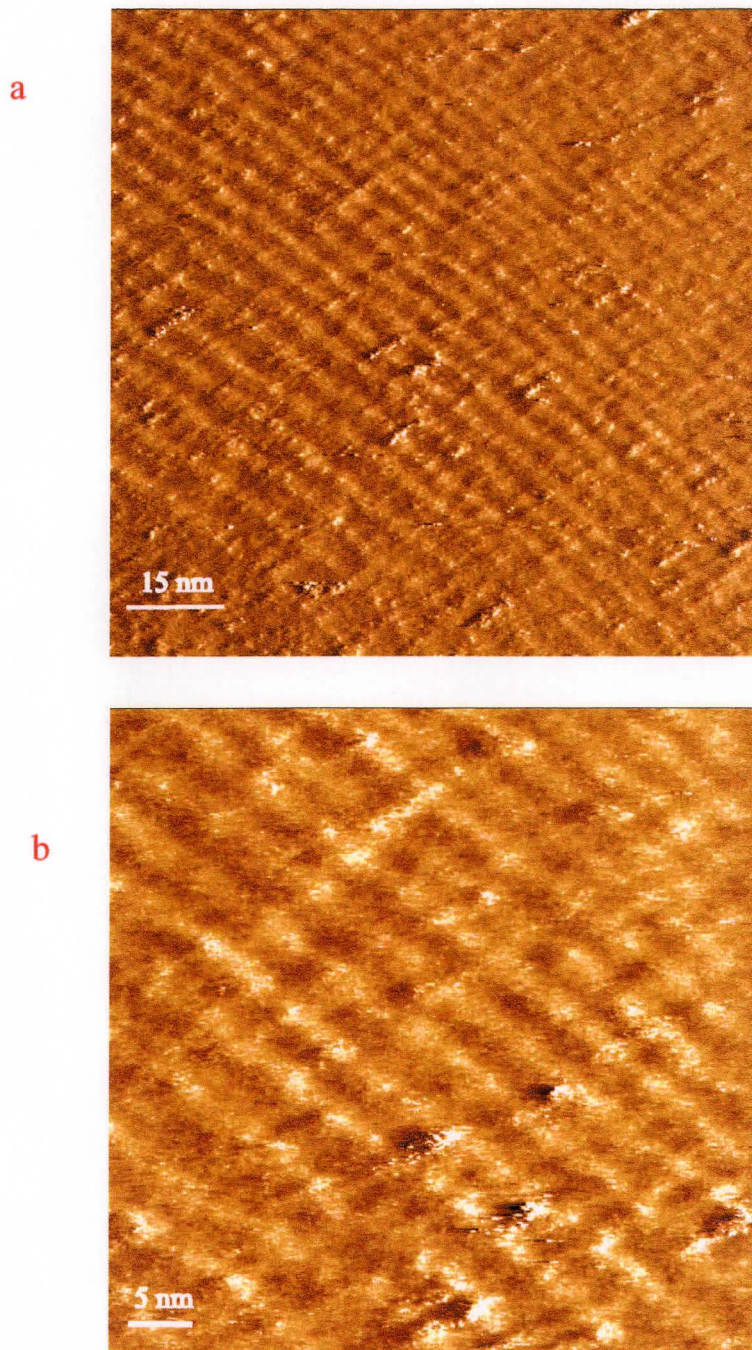


Figure 3-13 The STM images of the mixture between CuPcSC<sub>5</sub> with stearic acid on Au(111)

each row is composed of several bright spots, which should be  $\text{CuPcSC}_5$  molecules. However, no individual molecules are resolved in the STM image. The reason might be that the molecules are too close to each other. In addition, the movement of molecules on the surface also caused the difficulty in imaging the  $\text{CuPcSC}_5$  molecules.

### 3.5.8 The structure of the molecules after annealing the sample

After the sample of the  $\text{CuPcSC}_5$  monolayer was heated for 3 h at  $150^\circ\text{C}$ , the very ordered pattern is formed in the small area as circles by the white rings in Figure 3-14. The spots are arranged in the different directions. However, the size of the spots is bigger than the gold atom and smaller than the molecules. The nature of this spots is unclear at this point.

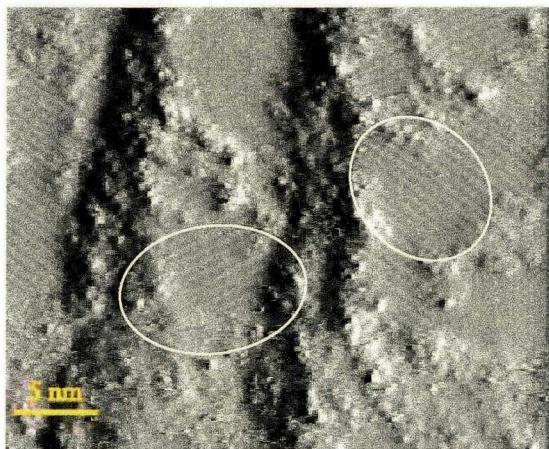


Figure 3-14 The annealed sample of  $\text{CuPcSC}_5$ .  $I_t = 0.2 \text{ nA}$ ,  $V_B = 1099.85 \text{ mV}$

Another image of the new prepares sample of  $\text{CuPcSC}_5$  was taken after annealing the sample for a few hours as shown in Figure 3-15. Molecules are formed into bands with protrusion. The distance between bands is about 5 nm smaller than the distance in the sample without heating. It might be the reason that the heating increases the energy of molecules, which assists molecules to close to each other.

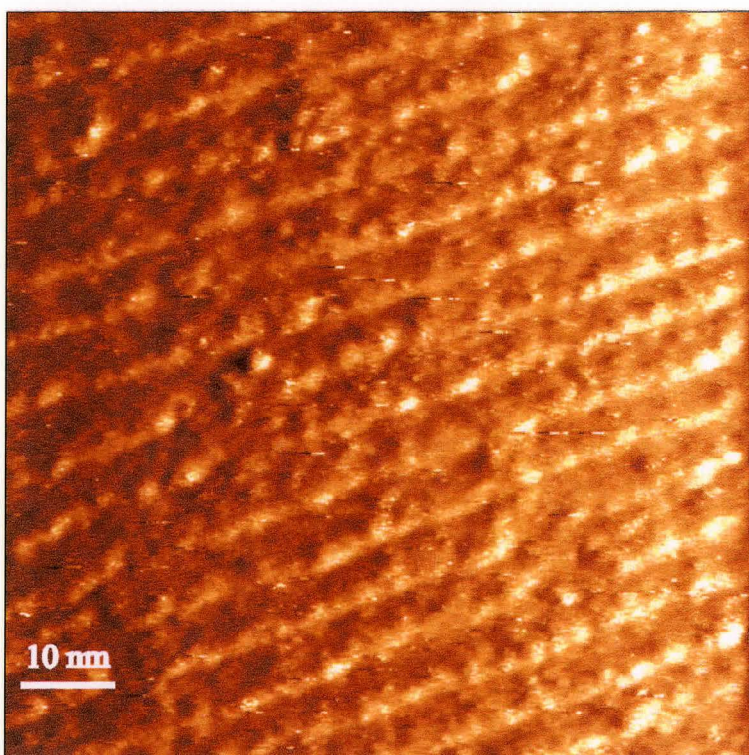


Figure 3-15 The STM image of the annealed sample of  $\text{CuPcSC}_5$  on Au(111)

### 3.6 Conclusions

Through using three methods to prepare the films of  $\text{CuPc}$ ,  $\text{CuPcSC}_5$  and

CuPcSC<sub>8</sub> on the Au(111) surface, the orientations of those molecules are investigated with STM. It was found that most of the structures of molecules are induced by the STM tip. The interaction between molecules and the gold surface is very weak, even the sulfur atoms are introduced into molecules. Compared the structure of CuPc without any alkyl chain, CuPcSC<sub>5</sub> and CuPcSC<sub>8</sub> have much possibility to form the ordered structure with the self-assembled method. However, it is difficult to determine the orientation of molecules due to the movement of molecules on the gold surface. The molecules in the Langmuir-Blodgett films did not form a regular pattern and the structures of molecules are still affected by the STM tip. CuPcSC<sub>5</sub> and CuPcSC<sub>8</sub> molecules tend to arrange themselves into a rod-like shape due to the  $\pi$ - $\pi$  interaction between molecules. Through annealing the prepared sample, the molecules probably change their structure to form a regular pattern. In addition, we also found that with the length of the substituted alkyl chains decreasing, the molecules more easily formed the ordered structure.

During this project, the lack of high-resolution STM images leads to a difficulty in determining the molecular orientation. One way to get informative images is to increase the interaction between the molecules and the substrate through changing thio-ether group into thio group. However, the replacement of thio group will cause polymerization between molecules. This is the reason that we chose thio-ether group in

the first place. In the next step, we can try to make thio group react with other group to protect thio group. After the molecules are adsorbed on the gold surface, the protective groups will detach from the thio group. Then, the formation of the chemical bond between the sulfur atom and the gold surface will assist the molecules to anchor on the surface. Another way is to mix CuPcSC<sub>5</sub> or CuPcSC<sub>8</sub> with other molecules such as stearic acid. The molecules with long chains have a strong interaction with the CuPcSC<sub>5</sub> or CuPcSC<sub>8</sub> molecules. The effect is to increase the interaction between molecules. It also increases the contact area between molecules and the substrate. The interaction between molecules and the substrate is strengthened, leading to the increasing probability to form a regular pattern of molecules.

## References

1. Berezin BD, Vopian VG. Coordination compounds of porphyrins and phthalocyanines. New York: Wiley; 1981. 1-37 p.
2. Moser FH, Thomas AL. Phthalocyanine compounds. New York: Reinhold Publishing Corporation; 1963. 1-45 p.
3. Rella R, Serra A, Siciliano P, Tepore A, Valli L, Zocco A. Langmuir-Blodgett multilayers based on copper phthalocyanine as gas sensor materials: active layer-gas interaction model and conductivity modulation. *Langmuir* 1997;13:6562-

- 6567.
4. Van Slyke SA, Chen CH, Tang CW. Organic electroluminescent devices with improved stability. *Appl. Phys. Lett.* 1996;69:2160-2162.
  5. Parthasarathy G, Burrows PE, Khalfin V, Kozlov VG, Forrest SR. A metal-free cathode for organic semiconductor devices. *Appl. Phys. Lett.* 1998;72:2138-2140.
  6. Eichhorn H, Bruce DW, Wöhrle D. Amphitropic mesomorphic phthalocyanines - a new approach to highly ordered layers. *Adv. Mater.* 1998;10:419-422.
  7. Mizutani W, Shigeno M, Sakakibara Y, Kajimura K, Ono M, Tanishima S, Ohno K, Toshima N. Scanning tunneling spectroscopy study of adsorbed molecules. *J. Vac. Sci. Technol. A* 1990;8:675-678.
  8. Wang SD, Dong X, Lee CS, Lee ST. Orderly growth of copper phthalocyanine on highly oriented pyrolytic graphite (HOPG) at high substrate temperatures. *J. Phys. Chem. B* 2004;108:1529-1532.
  9. Chizhov I, Scoles G, Kahn A. The influence of steps on the orientation of copper phthalocyanine monolayers on Au(111). *Langmuir* 2000;16:4358-4361.
  10. Lu X, Hipps KW, Wang XD, Mazur U. Scanning tunneling microscopy of metal phthalocyanines: d7 and d9 Cases. *J. Am. Chem. Soc.* 1996;118:7197-7202.
  11. Qiu X, Wang C, Zeng Q, Xu B, Yin S, Wang H, Xu S, Bai C. Alkane-assisted adsorption and assembly of phthalocyanines and porphyrins. *J. Am. Chem. Soc.* 2000;122:5550-5556.
  12. Smolenyak P, Peterson R, Nebesny K, Tolrker M, O'Brien DF, Armstrong NR. Highly ordered thin films of octasubstituted phthalocyanines. *J. Am. Chem. Soc.* 1999;121:8628-8636.
  13. Boden N, Bushby RJ, Martin PS. Triphenylene-based discotic liquid crystals as

- self-assembled monolayers. *Langmuir* 1999;15:3790-3797.
14. Suto K, Yoshimoto S, Itaya K. Two-dimensional self-organization of phthalocyanine and porphyrin: dependence on the crystallographic orientation of Au. *J. Am. Chem. Soc.* 2003;125:14976-14977.
  15. Lei SB, Yin SX, Wang C, Wan LJ, Bai CL. Modular assembly of alkyl-substituted phthalocyanines with 1-Iodooctadecane. *Chem. Mater.* 2002;14:2837-2838.
  16. Hips KW, Scudiero L, Barlow DE, Cooke JMP. A self-organized 2-dimensional bifunctional structure formed by supramolecular design. *J. Am. Chem. Soc.* 2002;124:2126-2127.
  17. Zheng XY, Zhu WQ, Wu YZ, Jiang XY, Sun RG, Zhang ZL, Xu SH. *Displays* 2003;24:121-124.
  18. Tadayyon SM, Grandin HM, Griffiths K, Norton PR, Aziz H, Popovic ZD. CuPc buffer layer role in OLED performance: a study of the interfacial band energies. *Org. Electron.* 2004;5:157-166.
  19. Davidson K, Jones R, McDouald S. Controlled orientation of Langmuir-Blodgett films of substituted phthalocyanines. *Synth. Met.* 2001;121:1399-1400.
  20. Eichhorn H, Wohrle D, Pressner D. Glasses of new 2,3,9,10,16,17,23,24-octasubstituted phthalocyanines forming thermotropic and lyotropic discotic mesophases. *Liq. Cryst.* 1997;22:643-65.

## Chapter 4

### Introduction to single-walled carbon nanotubes and sidewall functionalization

#### 4.1 History of carbon nanotubes (CNTs)

More than thirty years ago, it was found that the decomposition of hydrocarbons at high temperatures in the presence of transition metal catalyst particles produced carbon filaments with less than 10 nm diameter.<sup>5</sup> However, no detailed studies of the thin filaments were performed until carbon nanotubes were discovered by Iijima in 1991.<sup>2</sup> He used TEM to observe graphitic carbon needles grown on the negative end of the carbon electrode used in the d.c. arc-discharge evaporation of carbon. High-resolution electron micrographs reveal that coaxial tubes of graphitic sheets are composed of needles as shown in Figure 4-1, ranging from 4 to 30 nm in diameter. It was the first time to confirm the existence of Multi-Walled Carbon Nanotubes (MWCNTs).

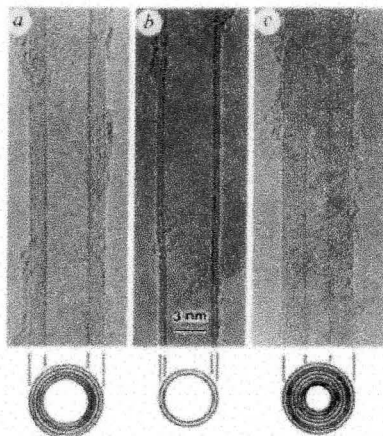


Figure 4-1 TEM images of multi-walled carbon nanotubes (a) five graphitic sheet tube, diameter 6.7 nm (b) two graphitic sheet tube, diameter 5.5 nm (c) seven graphitic sheet tube, diameter 6.5 nm.<sup>2</sup>

After that, the nanocapillarity of carbon nanotubes was calculated.<sup>8</sup> The electronic structure,<sup>9</sup> energetics<sup>10</sup> and metallic properties of graphene tubules<sup>11</sup> were discussed. However, those predictions are all on the basis of single-shell tubes. Less than two years later, Iijima and his coworker found that the single-walled carbon nanotubes (SWCNTs) were formed in soot-like deposits in the carbon-arc chamber in the presence of an iron catalyst.<sup>1</sup> The diameters of SWCNTs range from about 0.7 nm to 1.6 nm. The electron micrograph (Figure 4-2) showed that one single-shell tube with the diameter about 1.37 nm is attached to the nanotube bundles.

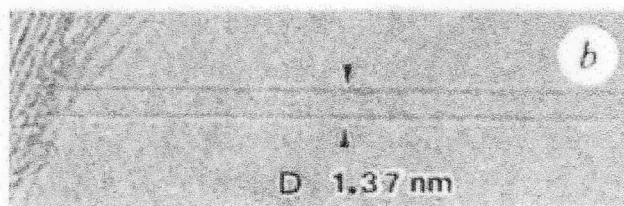


Figure 4-2 Electron micrograph of a single-shell carbon nanotube with the diameter about 1.37 nm.<sup>1</sup>

During the same period, Bethune and coworkers observed that SWCNTs with the diameter  $1.2 \pm 0.1$  nm are ubiquitous in the presence of cobalt catalyst.<sup>12</sup> After that, many efforts were made to improve the purity and the yield of SWCNTs. In 1996, Smalley and coworkers succeeded in synthesizing bundles of single-walled carbon nanotubes with nearly uniform diameter and obtained a good yield of SWCNTs. This enabled various research work to be carried out.<sup>13</sup> As one-dimensional conductors,<sup>14</sup> the uniqueness of SWCNTs attracts many interests due to their electronic structure and applications. In order to understand carbon nanotubes well, it is important to learn the basic background of SWCNTs.

## 4.2 Structure of CNTs

A SWCNT can be described as an extended fullerene molecule or as a graphene tubule with a constant diameter by rolling up one single graphene sheet into a cylinder as

shown in Figure 4-3.<sup>3</sup>

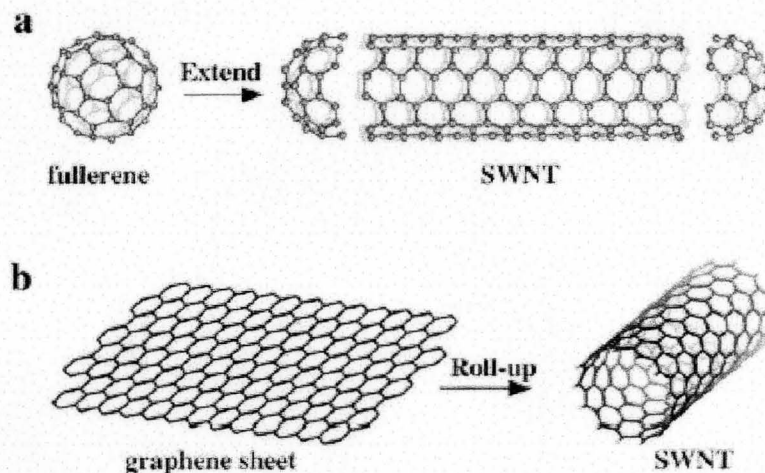


Figure 4-3 Schemes of a SWCNT: (a) an extended fullerene molecule with the diameter 0.7 nm (b) a graphene tubule by rolling up one single graphene sheet in to a cylinder.<sup>3</sup>

As early as in 1992, the calculations about SWCNTs suggested that they can be metallic or semiconducting.<sup>14</sup> Some of them have chirality. Their electronic structures depend on the diameter of the nanotube and the helicity sensitively. Those predictions were validated by experiments with scanning tunneling microscopy (STM) and scanning tunneling spectroscopy (STS) on individual single-wall nanotubes.<sup>6,7</sup>

A SWNT can be assumed that one single atomic layer of graphite with the honeycomb lattice is wrapped up into a seamless cylinder. The structure of a defect-free single-walled carbon nanotube is defined by the vectors  $C_h$  and  $T$  according to its

1D unit cell in Figure 4-4.<sup>6,7</sup>

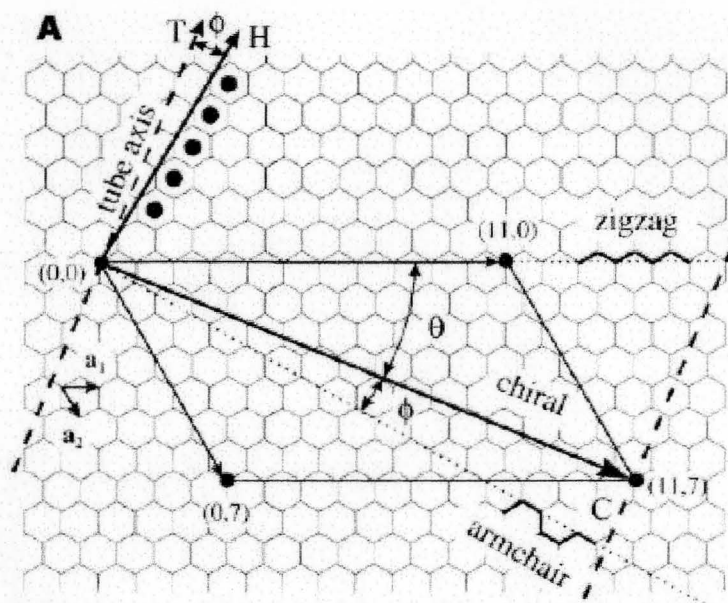


Figure 4-4 The construction of a SWCNT from a single graphene sheet.<sup>6,7</sup>

The wrapping vector  $C_h$  connects two crystallographically equivalent sites on a 2D graphene sheet, expressed by  $C_h = n\mathbf{a}_1 + m\mathbf{a}_2 \equiv (n, m)$ . In the formula,  $\mathbf{a}_1$  and  $\mathbf{a}_2$  are the graphene lattice vectors and  $n$  and  $m$  are integers. If  $n$  equals  $m$ , a tube is called “armchair”. If  $m$  equals zero, a tube is called “zigzag”. The chiral angle  $\theta$  is the angle between the “zigzag” direction and the  $C_h$  vector. The “zigzag” and “armchair” nanotubes have the chiral angles of  $\theta = 0$  and  $30^\circ$ , respectively. The chiral nanotubes have the chiral angles  $0 < \theta < 30^\circ$ . In addition, it was found that when  $n - m = 3l$  (where  $l$  is an integer), the tube will be metallic. If  $n - m \neq 3l$ , the tubes will be semiconducting.

All the armchair nanotubes are metallic. The zigzag nanotubes can be metallic or semiconducting.

#### 4.3 Studies of SWCNTs with STM and STS in the references

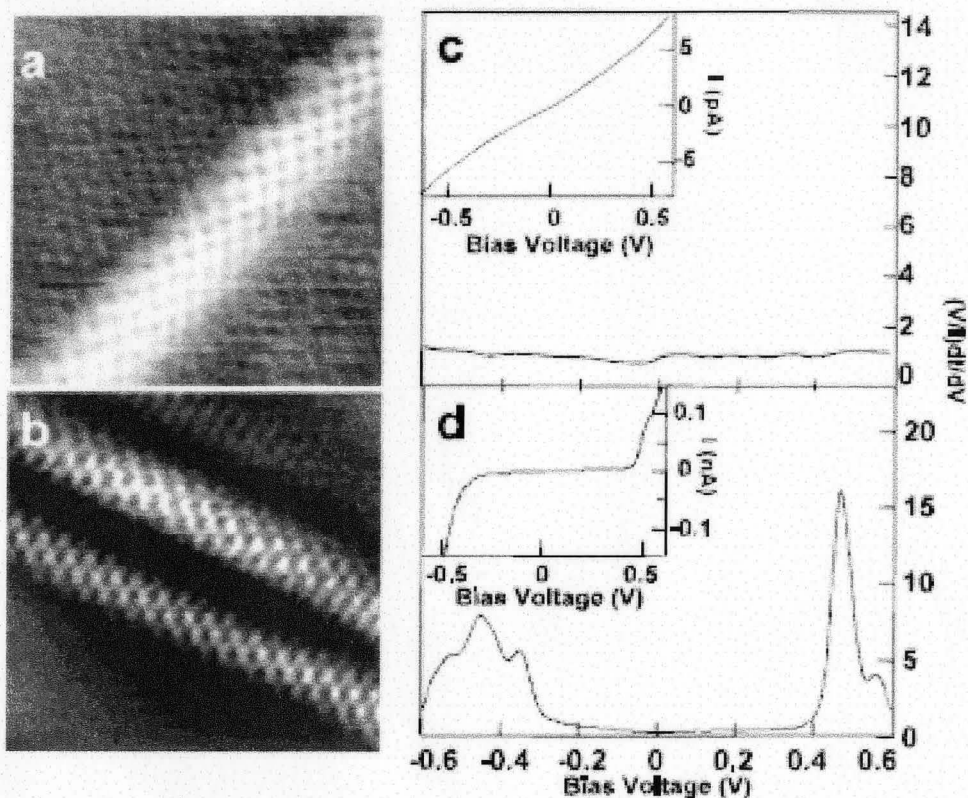


Figure 4-5 (a, b) STM images of isolated SWCNTs on Au(111).

(c, d) Calculated normalized conductance,  $(V/I)dI/dV$  and measured I-V (inset) recorded on the nanotube in a, b.<sup>4</sup>

The STM provides an effective way to determine the structure of carbon nanotube. The atomic resolution STM images of isolated SWCNTs on the Au(111) surface appear a honeycomb lattice like graphene sheet as shown in Figure 4-5 a and

b.<sup>4</sup>

Through measuring chiral angle and diameter of the tube in Fig. 5a, the  $(n, m)$  indices can be proposed as either  $(12, 3)$  or  $(13, 3)$ . However, a  $(12, 3)$  tube is metallic and a  $(13, 3)$  tube is semiconducting. It means that the electronic property of a tube can not be determined only through the STM image. The same nanotube was used to conduct scanning tunneling spectroscopy (STS). The local density of states is finite and constant between  $-0.6$  V and  $+0.6$  V in Figure 4-5c, which is the characteristic of a metal. The nanotube was finally determined to be of the  $(12, 3)$  type. In contrast to the tube in Figure 4-5a, the tube in Figure 4-5b is predicted to be the  $(14, -3)$  type from the STM image. The tube should exhibit the semiconducting characteristic. From the I-V curve in Figure 4-5d, the band gap is very clearly present but the LDOS sharply increases at  $-0.325$  and  $+0.425$  V. It is consistent with the characteristic of the conduction and valence bands of a semiconductor. The tube in Figure 4-5b is determined to be semiconducting, which has a chirality opposite to the tube in Figure 4-5a.

Although the determination of the electronic structures of SWCNTs is resolved with STM, separating SWCNTs in the rope and dissolving them in organic solvent or water are still active area of research. SWCNTs consist purely of  $sp^2$ -hybridized carbon

atoms to form a large  $\pi$ - $\pi$  conjugated system which provides them with excellent conductivity. However, it also causes them to preferentially aggregate into bundles with different diameters. Those problems prevent the applications of SWCNTs in many fields. Functionalization of SWCNTs is a probable method to improve solubility and combine the unique properties of SWCNTs with those of other types of materials.<sup>15</sup> Several approaches have been developed to functionalize SWCNTs, such as defect functionalization,<sup>16,17</sup> covalent functionalization of the sidewall, noncovalent functionalization of CNTs wrapped with a conjugated polymer.<sup>18</sup> Among them, chemical functionalization is a very important method to attach functional groups on nanotubes.

#### 4.4 Functionalization of SWCNTs

It is known that a nanotube is an  $sp^2$ -hybridized carbon atom network. As an  $sp^2$ -hybridized (trigonal) carbon atom, it strongly prefers planarity. After chemical functionalization, an  $sp^2$ -hybridized (trigonal) carbon atom in nanotubes is converted into an  $sp^3$ -hybridized (tetrahedral) carbon atom due to the attachment of functional group, which relieves the strain at the point of attachment. However, if several functional groups are attached on the nanotube in the neighboring area, they will cause new strain because most of carbon atoms around  $sp^3$ -hybridized (tetrahedral) carbon atoms prefer a planar

geometry. The attachment of several functional groups in the neighboring area has a larger influence on the neighboring carbon atoms than that of one functional group. In the reference, it is reported that on the fluorinated nanotube the bond energy of a second carbon-fluorine bond is highest when the bond forms adjacent to the first.<sup>19</sup> The relief of strain will increase the reaction to saturate carbon atoms after a proper number of functional groups are attached in the neighboring area. Therefore, the end caps of CNTs with a large curvature are more reactive than the sidewall of CNTs. A highly reactive reagent must be used to chemically functionalize the nanotube sidewalls. In addition, the existence of the defect sites located on the sidewalls,<sup>20</sup> such as five or seven-membered rings or vacancy of carbon atoms, increases the possibility to functionalize the nanotube sidewall. Those defects, which have a higher reactivity compared with other points of nanotube, can serve as a starting point for the covalent chemical functionalization of SWCNTs. After chemical functionalization, the electronic properties of CNTs might be changed from metallic to semiconducting. Although a few methods, such as TEM, SEM and AFM, are extensively used to characterize the functionalized CNTs, the resolution of the images is not enough to discriminate functional groups on nanotube. After Lieber<sup>7</sup> et al. and Dekker et al.<sup>6</sup> resolved the hexagonal-ring structure of the nanotube wall and explored the electronic properties of nanotube related to the diameter and helicity of

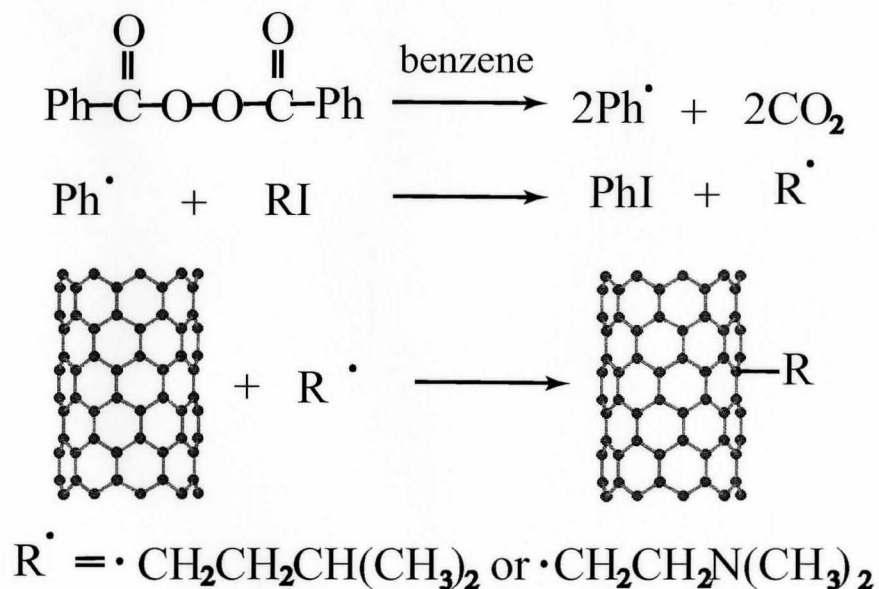
nanotube with scanning tunneling microscopy (STM), more efforts will be paid to study the alignment of functional groups and the properties of the functionalized SWCNTs with STM.

#### 4.5 Introduction of my project

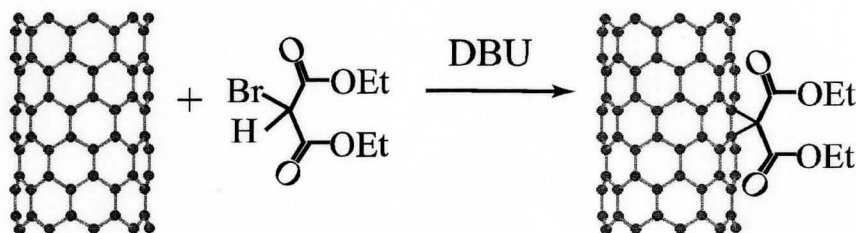
Here, we report the investigation of the functionalized carbon nanotubes by free radicals and via the Bingel reaction. The functionalized carbon nanotubes were synthesized according to the methods reported by Billups's group<sup>21</sup> and Coleman's group.<sup>22</sup> Kimberly Worsley, a former undergraduate student in our lab, functionalized the SWCNTs by free radicals<sup>21</sup> and via the Bingel reaction.<sup>22</sup> The procedures of synthesis are described as scheme 4-1 and 4-2. In scheme 4-1 and 4-2, the structure of nanotubes was optimized with molecular mechanics method at a MM+ level by software HyperChem 6.0 version.

In our previous work, Worsley<sup>23</sup> reported the long-range periodicity in carbon nanotube sidewall functionalization with the Bingel reaction. Functional groups are aligned along a number of nanotubes with different space periodicity under various conditions. This phenomenon has caused some interests. Li et al. reported that polymer single crystals were decorated onto both SWCNTs and MWCNTs with 20-70 nm under

the control of crystallization conditions.<sup>24</sup> Although the mechanism to form the periodicity of functional groups on CNTs by the Bingel reaction is different from that to form the periodicity of polymer single crystals on CNTs, it is necessary to find the reason of forming periodicity, which will be helpful to control the pattern of functional groups on CNTs in the future. In the paper, we report the properties of SWCNTs functionalized by the free radical reaction and the Bingel reaction on the highly oriented pyrolytic graphite (HOPG) surface.



Scheme 4-1 Functionalization of SWCNTs by free radicals



Scheme 4-2 Functionalization of SWCNTs via the Bingel reaction

## References

1. Iijima S, Ichihashi T. Single-shell carbon nanotubes of 1-nm diameter. *Nature* 1993;363:603-605.
2. Iijima S. Helical microtubules of graphitic carbon. *Nature* 1991;354:56-58.
3. Odom TW, Huang JL, Lieber CM. STM studies of single-walled carbon nanotubes. *J. Phys.: Condens. Matter* 2002;14:R145-167.
4. Odom TW, Huang JL, Kim P, Lieber CM. Structure and electronic properties of carbon nanotubes. *J. Phys. Chem. B* 2000;104,:2794-2809.
5. Oberlin A, Endo M, Koyama T. High-resolution electron-microscope observations of graphitized carbon-fibers. *Carbon* 1976;14:133-135.
6. Wildoer JWG, Venema LC, Rinzler AG, Smalley RE, Dekker C. Electronic structure of atomically resolved carbon nanotubes. *Nature* 1998;391:59-62.
7. Odom TW, Huang JL, Kim P, Lieber CM. Atomic structure and electronic properties of single-walled carbon nanotubes. *Nature* 1998;391:62-64.
8. Pederson MR, Broughton JQ. Nanocapillarity in fullerene tubules. *Phys. Rev. Lett.* 1992;69:2689-2692.

9. Saito R, Fujita M, Dresselhaus G, Dresselhaus MS. Electronic structure of chiral graphene tubules. *Appl. Phys. Lett.* 1992;60:2204-2206.
10. Robertson DH, Brenner DW, Mintmire JW. Energetics of nanoscale graphitic tubules. *Phys. Rev. B* 1992;45:12592-12595.
11. Mintmire JW, Dunlap BI, White CT. Are fullerene tubules metallic. *Phys. Rev. Lett.* 1992;68:631-634.
12. Bethune DS, Kiang CH, Devries MS, Gorman G, Savoy R, Vazquez J, Beyers R. Cobalt-catalysed growth of carbon nanotubes with single-atomic-layer walls. *Nature* 1993;363:605-607.
13. Thess A, Lee R, Nikolaev P, Dai H, Petit P, Robert J, Zu C, Lee YH, Kim SG, Rinzler AG and others. Crystalline ropes of metallic carbon nanotubes. *Science* 1996;273:483-487.
14. Hamada N, Sawada S, Oshiyama A. New one-dimensional conductors: graphitic microtubules. *Phys. Rev. Lett.* 1992;68:1579-1581.
15. Hirsch A. Functionalization of single-walled carbon nanotubes. *Angew. Chem. Int. Ed.* 2002;41:1853-1859.
16. Chen J, Hamon MA, Hu H, Chen Y, Rao AM, Eklund PC, Haddon RC. Solution properties of single-walled carbon nanotubes. *Science* 1998;282:95-98.
17. Hamon MA, Chen J, Hu H, Chen YS, Itkis ME, Rao AM, Eklund PC, Haddon RC. Dissolution of single-walled carbon nanotubes. *Adv. Mater.* 1999;11:834-840.
18. Star A, Stoddart JF, Steuerman D, Diehl M, Boukai A, Wong EW, Yang X, Chung SW, Choi H, Heath JR. Preparation and properties of polymer-wrapped single-walled carbon nanotubes. *Angew. Chem. Int. Ed.* 2001;40:1721-1725.
19. Bauschlicher Jr. CW. Hydrogen and fluorine binding to the sidewalls of a (10, 0) carbon nanotube. *Chem. Phys. Lett.* 2000;322:237-241.

20. Mawhinney DB, Naumenko V, Kuznetsova A, Yates JT, Liu J, Smalley RE. Surface defect site density on single walled carbon nanotubes by titration. *Chem. Phys. Lett.* 2000;324:213-216.
21. Ying Y, Saini RK, Liang F, Sadana AK, Billups WE. Functionalization of carbon nanotubes by free radicals. *Org. Lett.* 2003;5:1471-1473.
22. Coleman KS, Bailey SR, Fogden S, Green MLH. Functionalization of single-walled carbon nanotubes via the Bingel reaction. *J. Am. Chem. Soc.* 2003;125,:8722-8723.
23. Worsley KA, Moonosawmy KR, Kruse P. Long-range periodicity in carbon nanotube sidewall functionalization. *Nano Lett.* 2004;4:1541-1546.
24. Li CY, Li L, Cai W, Kodjie SL, Tenneti KK. Nanohybrid Shish-Kebabs: periodically functionalized carbon nanotubes. *Adv. Mater.* 2005;17:1198-1202.

## Chapter 5

### Sidewall functionalization of single-walled carbon nanotubes

#### 5.1 Introduction

In this chapter, it mainly introduced the results of sidewall functionalization of SWCNTs by free radicals and via the Bingel reaction with STM. Through our observation, some interesting phenomena such as correlation between nanotubes are observed. The probable reasons were discussed on the basis of analyzing the STM images.

#### 5.2 Experimental section

The raw SWCNTs were purchased from Carbon Nanotechnologies Inc., TX. and were produced by the HiPco process. The functionalization of SWCNTs by free radicals or via the Bingel reaction was performed as described in the references.<sup>1, 2</sup> All synthetic work described in this section was done by Kim Worsley, a former undergraduate student in our lab.

The functionalization of SWCNTs by free radicals is as follows. First, the 20 mg unshortened SWCNTs without further purification were added to 30 mL of benzene and

sonicated for 30 min in a 50 mL flame dried round-bottom flask. Then the 4.0 mmol alkyl iodide and 1.6 mmol benzoyl peroxide were added to this suspension. The reaction proceeded at 75 °C for 24 h with stirring. The whole system was filled with argon. After 24 h, the mixture in the flask was diluted with 100 mL of benzene, then filtered by a 0.2 µm PTFE paper and washed extensively with benzene. After this, the paper was allowed to dry at room temperature in air overnight. In this experiment, the alkyl iodide is isopentyl iodide or 2- (N, N-dimethyl) amide-1-ethyl iodide. The SWCNTs were functionalized with isopentyl groups or 2- (N, N-dimethyl) amide-1-ethyl groups.

The procedure to functionalize SWCNTs via the Bingel reaction was described in our previous paper.<sup>3</sup> The unshortened SWCNTs were added to 15 mL of *o*-dichlorobenzene in a 50 mL dry flask. After sonication for 20 min, 0.5 mL of 1,8-diazabicyclo[5.4.0]undec-7-ene (DBU) and 0.3 mL of diethylbromomalonate were added to this suspension. This mixture was stirred for 19 h without heating. Trifluoroacetic acid was added to the mixture to quench the Bingel reaction. After stirring for 5 min, this mixture was filtered with 0.2 µm PTFE paper and washed extensively ethanol. The paper coated with the functionalized SWNTs was dried at room temperature in air for one night.

A small amount of each kind of functionalized SWCNTs was suspended in

ethanol with sonication for more than 30 min. A drop of each suspension was added on a freshly peeled highly oriented pyrolytic graphite (HOPG) surface. After the solvent evaporated in air, the surfaces were imaged under ambient condition. The STM is Digital Nanoscope II (type A head). The STM tip is made from the Pt/Ir wire cut by sharp scissors.

## 5.3 Results and Discussion

### 5.3.1 Correlation between the nanotubes within the same bundle

High-purity bulk of SWCNTs tend to align themselves with each other to form bundles or ropes with the diameter 5 to 20 nm to maximize van der Waals contact and lower their energy.<sup>4,5</sup> After functionalization, steric hindrance resulting from bulk groups on the nanotube sidewall results in a decrease of the average diameter of SWCNT bundles. Here, we show the observation of the bundles with less than 10-nm diameter of SWCNTs functionalized by free radicals and via the Bingel reaction on the graphite surface. It was found that a correlation exists between nanotubes within the same bundle.

Similar to the interaction between graphite layers, the interaction between nanotubes and the graphite surface assists nanotubes to fix on the graphite surface,<sup>6</sup> which provide the possibility to image them with STM at ambient temperature. Figure 5-

1 shows the STM images of the bundles of SWCNTs functionalized by isopentyl radicals. The bundles appear the “raft”-like structures similar to the observation about the thin unfunctionalized CNT ropes on the Au(111) substrate reported by Odom and the coworkers.<sup>5</sup> Such structure increases the effective area of nanotube-substrate contact to minimize the energy of the thin bundle.<sup>7</sup> In Figure 5-1a, a few nanotube bundles were aligned parallel with each other. In the area marked by the letter **B**, two bundles with similar diameter are very close to each other. The bright dots with strong color contrast are aligned on both of the bundles. Compared with the STM images of clean nanotubes reported in the references,<sup>8-10</sup> the bright dots are attributed to be isopentyl groups. Through carefully observing the features of each bundle, the correlation between the bundles was found as marked by the parallel arrows between two bundles. The areas on each bundle pointed by the same arrow have the similar functionalized degree. The same phenomenon occurs on the two bundles with smaller diameter aligned in the area marked by the letter **A**. Although the bundles in the area **A** are far away from those in the area **B**, the correlation still exists between the bundles in the different area marked by the longer parallel arrows. The features on each bundle in the same area are not the completely same as each other, which excludes the possibility that the bundles are artifacts formed by the double tips. The correlation between the different bundles suggests that they should be

from the same large bundle when they were in the suspension. During the process to deposit it on the graphite surface, the large bundle was divided into a few small bundles as illustrated by Figure 5-1b. The driving force might be the interaction between the bundles and the graphite surface. The weak interaction between nanotubes after functionalization also plays an important role in breaking the large bundle. From the bundles in the area A, we found that the unfunctionalized segments of the nanotube appear as the very thin lines. They alternate with the functionalized segments, consistent with the results from the fluorinated nanotube sidewalls reported by Halas and his coworkers.<sup>11</sup> In the area circled by one dashed ring in Figure 5-1a, some large particles staying on the bundles might be the impurity produced during the synthesis of nanotubes, such as fullerenes or the metal catalyst, which were absorbed on the nanotubes especially on the highly functionalized segments of nanotubes.

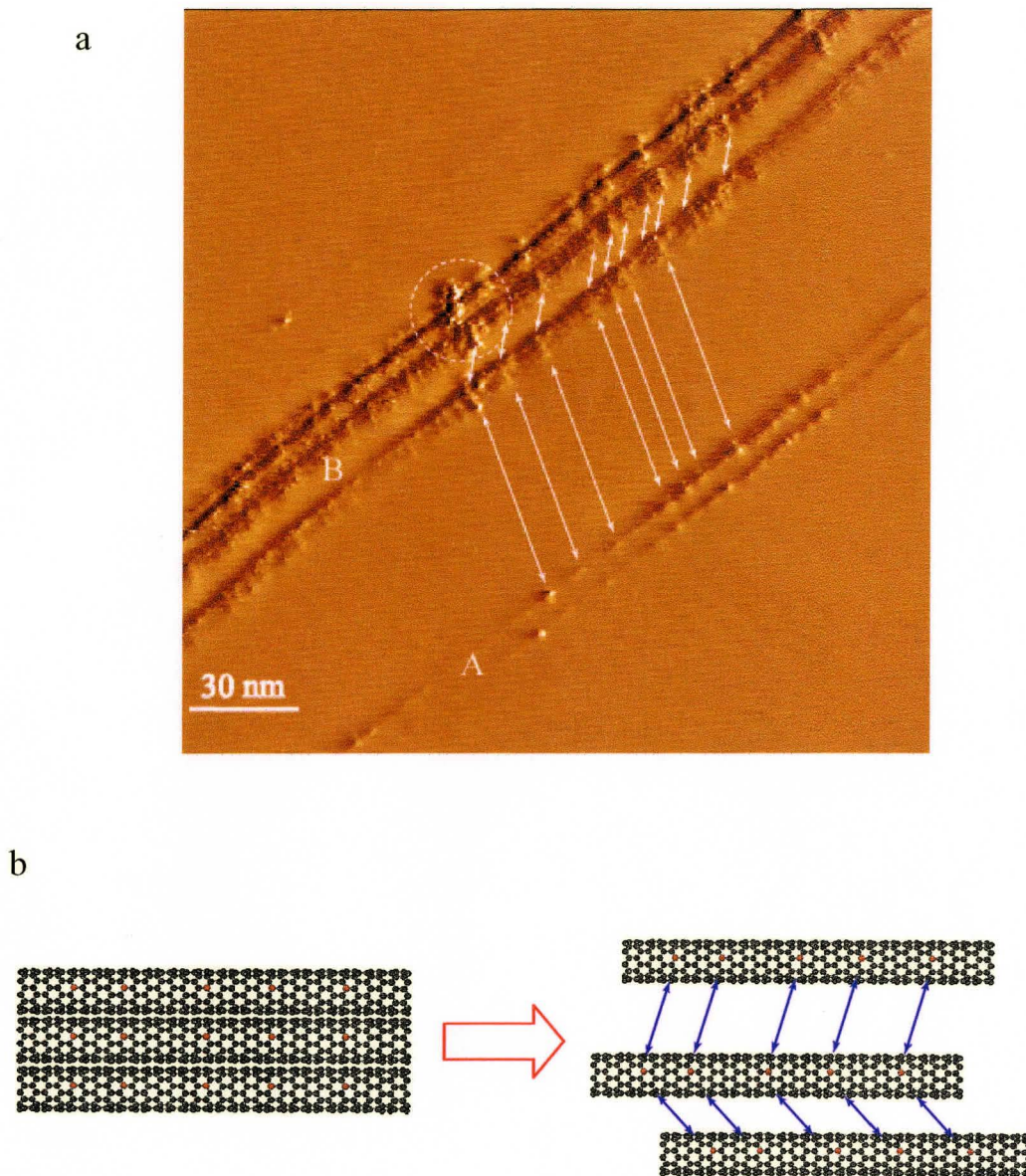
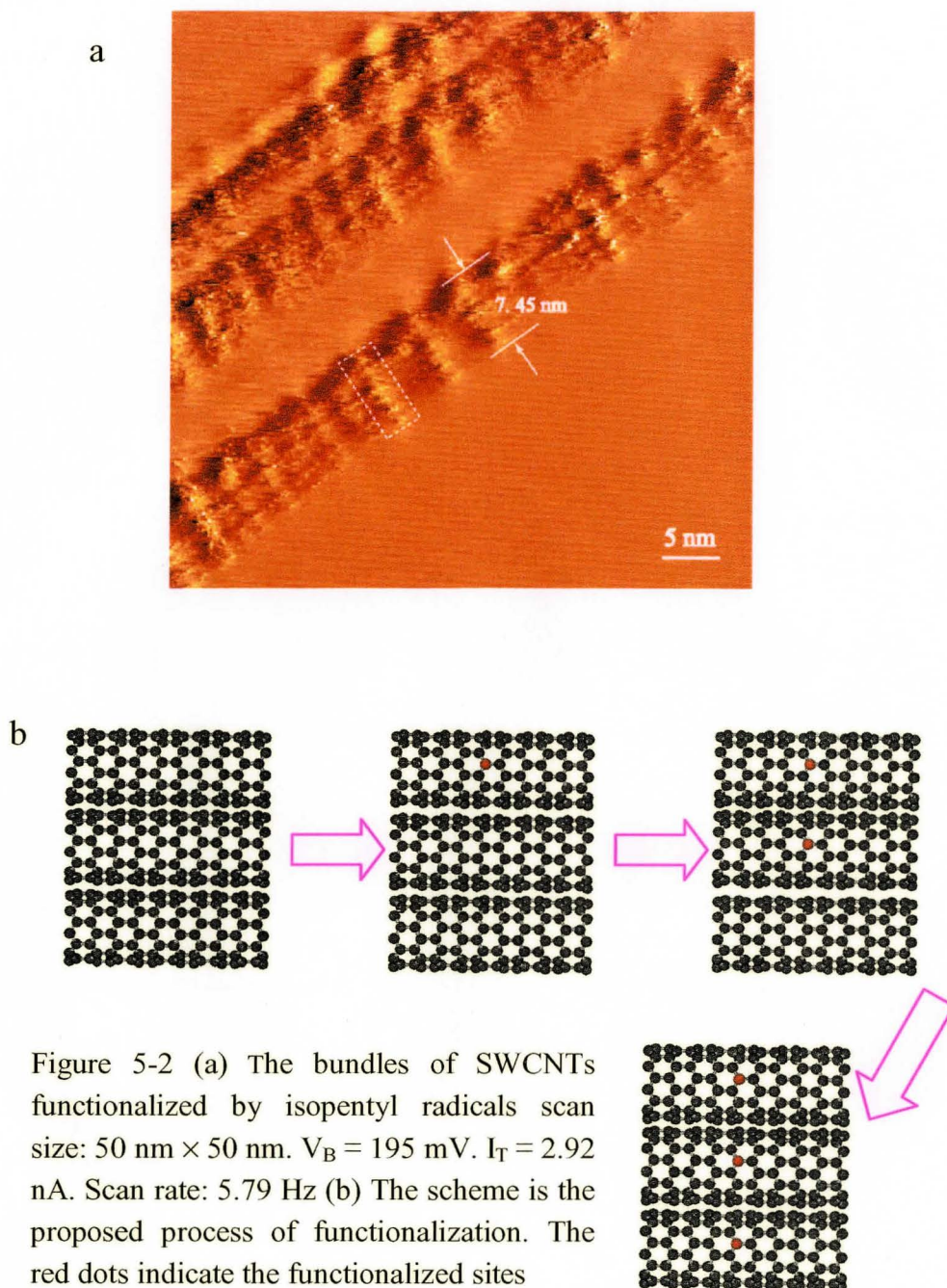


Figure 5-1a The bundles of SWCNTs functionalized by isopentyl radicals

scan size:  $203 \text{ nm} \times 203 \text{ nm}$ .  $V_B = 100 \text{ mV}$ .  $I_T = 1.5 \text{ nA}$ . Scan rate:  $3.47 \text{ Hz}$ .

b The scheme is the proposed process of the bundle break. The red dots indicate the functionalized sites



Choosing a small area to image from Figure 5-1a, the STM image with high magnification as shown in Figure 5-2a was captured from the bundles aligned in the area

**B** in Figure 5-1a. More information about the bundles was revealed in Figure 5-2a. Each bundle is composed of a few nanotubes, maybe four or five nanotubes, which can be counted from the lowest bundle in Figure 5-2a. The diameter of the lowest bundle is about 7.45 nm. Other bundles in Figure 5-2a are less than 10 nm in diameter. The correlation between nanotubes within each bundle can be observed. The functional groups aligned into a row perpendicular to the axis of the bundle as shown by the dashed rectangle frame. The functionalized degrees of the nanotubes in the same bundle are very similar to each other. Even the functional groups have the similar distribution on the nanotubes. This phenomenon can be explained from the process to functionalize SWNTs. Before functionalization, the bulk of SWNTs aggregated together to form ropes or bundles to decrease their energy. Lieber and his coworkers mentioned that within a tightly packed nanotube rope, the  $\pi$  and  $\pi^*$  bands of armchair (n, n) SWCNTs are allowed to mix resulting in a pseudogap at the Fermi energy.<sup>12</sup> It means that the electronic structures of nanotubes in the rope are affected by each other. The rope or the bundle of nanotubes can be considered as one macromolecule such as one large-diameter CNT during the process of functionalization. After one isopentyl radical attacks the carbon atom with lower electron density on one nanotube sidewall, one C-C bond of sidewall is opened and the produced lone electron is delocalized in the whole system of

the rope or the bundle. The covalent addition of functional group changed the electronic structure of the rope or the bundle. The electron density of each atom is not equivalent to each other after functionalization. The next free radical prefers to attack the neighboring nanotube and chooses the carbon atom at the same position as that of the bonded carbon atom by the first isopentyl radical because 1) the first functional group have the largest influence on the neighboring nanotube and 2) these two carbon atoms at the same position on different nanotube have the completely same electronic environment before functionalization. In this mechanism of functionalization, the next site to be attacked by the free radical would be prescribed. After all the atoms at the same position on different nanotubes within the same rope or the bundle are bonded by free radicals as shown in Figure 5-2b, the next isopentyl radical will choose the carbon atom with lowest electron density at the different position to bond. The same mechanism of functionalization will repeatedly work on the carbon atoms at the same position on different nanotubes. The route of functionalization will be recycled until the reaction is terminated. During our previous study, we ever observed the similar correlation between nanotubes functionalized via the Bingel reaction. However, we did not find a good explanation for those cross-correlations at that time.<sup>3</sup>

In Figure 5-2a, we noticed that the distance between two neighboring rows is

different, which indicates that the functional groups might be aligned on some kinds of nanotubes without periodicity. It can be explained that the existence of defects, such as the five or seven membered ring and the vacancy of carbon atoms, leads to the carbon atoms with different reactivity in the same nanotube. The reaction prefers to choose the defects as the starting points. After the first functional group is bonded on the carbon atom at the defect site, it will affect the next covalent addition on the nanotube sidewall. A lot of defects exist on the nanotube sidewall, which leads to the irregular distribution of electron density. Such distribution of electron density decides the pattern of functional groups without periodicity.

We also observed the functionalized SWCNTs by the different radicals 2-(N, N-dimethyl) amide-1-ethyl radicals with STM on graphite. The similar correlation was found between the nanotubes. The STM images obtained from these nanotubes suggest that the large bundle was broken up during the process to deposit it on the graphite surface, which is similar to the observation of the functionalized SWCNTs by isopentyl radicals. Compared with isopentyl group, 2-(N, N-dimethyl) amide-1-ethyl group has the similar structure except that one carbon atom was replaced by one nitrogen atom. The size of 2-(N, N-dimethyl) amide-1-ethyl group is similar to the size of isopentyl group, which indicates that the steric hindrance from 2-(N, N-dimethyl) amide-1-ethyl group on

SCWNTs should be similar to that from isopentyl group. Due to the similar structures of these two different radicals, it is expected that they would have a similar reactivity to the same SWCNT. If the hypothesis is true, these two different functional groups will be aligned on the nanotubes with the same diameter and helicity in a similar pattern, respectively.

Here, the sidewall functionalization of SCWNTs via the Bingel reaction was also investigated on the graphite surface. Figure 5-3 exhibited the STM image obtained from the functionalized SWCNTs via the Bingel reaction. The functionalized segments of the nanotubes appear bright as shown in Figure 5-3. The distance between two



Figure 5-3 The SWCNTs functionalized via the Bingel reaction scan size: 20 nm  $\times$  20 nm.  $V_B = 20.14$  mV.  $I_T = 1$  nA. Scan rate: 19.53 Hz

neighboring groups is different. The functional groups are aligned on the nanotube sidewalls in an irregular pattern. In our previous study, we observed the same phenomenon. Both the long-range regular pattern with 4.6 nm periodicity and the irregular pattern were found on the SWCNTs functionalized via the Bingel reaction with stirring for 19 h.<sup>3</sup> In our previous paper, it was proposed that the attachment of the first functional group leads to the regular spatial fluctuations of electron density, then the regular pattern for subsequent covalent addition is prescribed.<sup>3</sup> The existence of irregular patterns indicates that a large proportional defects on the nanotube sidewall disturb the regular spatial fluctuations of electron density induced by the first functional group and the spatial distribution of electron density appears as an irregular pattern, which leads to the subsequent attachment of functional groups without periodicity. In addition, the cross-correlation between nanotubes was observed as shown by the parallel arrows in Figure 5-3. It is very similar to the correlation observed from the functionalized SWCNTs by free radicals. Compared with all the data we have, it can be concluded that the correlation extensively exists between functionalized nanotubes due to the mechanism of functionalization.

### 5.3.2 Periodicity of functional groups

In our previous work, we reported that the functional groups are aligned on some of SWCNTs functionalized via the Bingel reaction with 4.6 nm periodicity.<sup>3</sup> Here, the periodicities of functional groups are also found on some SWCNTs functionalized by free radicals.

The STM image as shown in Figure 5-4 is obtained from the functionalized SWCNTs by isopentyl radicals. One nanotube bundle, composed of a few nanotubes, appears as a bright band. Those nanotubes in the bundle might be functionalized by isopentyl radicals. However, the aggregation of nanotubes leads to the difficulty in discriminating the functional groups on SWCNTs. One or two nanotubes are found to

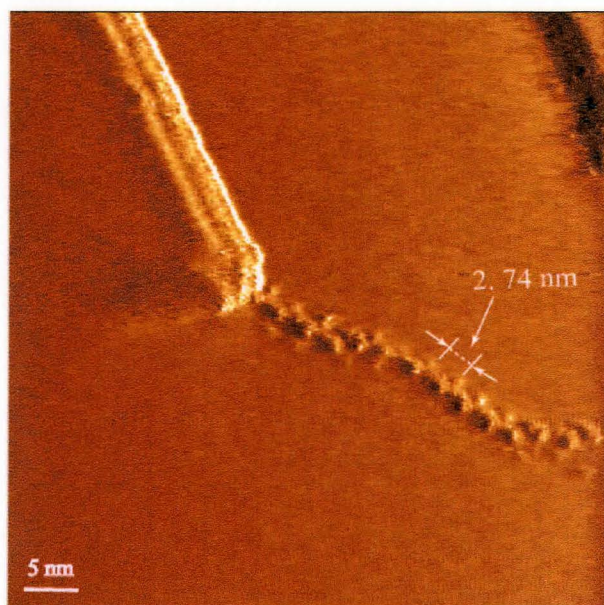


Figure 5-4 The functionalized SWCNTs by isopentyl radicals. Scan size: 43.6 nm  $\times$  43.6 nm.  $V_B = 124.8$  mV.  $I_T = 1.5$  nA. Scan rate: 5.79 Hz

be connected with the tail of the bundle. We speculated that during the process of functionalization, the radicals of SWCNTs collided with the tails of the other SWCNTs with one lone electron resulting in the termination of the reaction. The bright dots alternate with the dark segments along the nanotubes attached with the bundle. The bright dots are thought to be functional groups compared with our other images. The functional groups are aligned in a regular pattern with a periodicity about 2.74 nm on the SWCNTs. The attachment of functional groups produced the sp<sup>3</sup>-hybridized defects on SWCNTs leading to the break of the conjugated system of SWCNTs, which make unfunctionalized segments appear dark. In addition, we noticed that the functional groups can be resolved on the small bundle or on the individual SWCNTs. It suggests that the wave function of functional groups might overlap with each other in the nanotube bundle, which make difficult to determine the functional groups.

The periodicity of functional groups was also found on the SWCNTs functionalized by 2- (N, N-dimethyl) amide -1- ethyl radicals as shown in Figure 5-5. The periodicity did not appear on the all the nanotube bundles. In Figure 5-5, one nanotube bundle with functional groups aligned in a regular pattern crosses with other bundles. The diameter of the bundle with a regular pattern of functional groups is about 4.6 nm as shown by the dashed line. Three nanotubes, each of which possesses functional groups in

a similar periodicity form this bundle. In the image with higher magnification as shown in Figure 5-5b, the distance between two neighboring functional groups is measured about 1.2 nm, which is much smaller than the periodicity 4.6 nm on the nanotubes functionalized by the Bingel reaction observed by Worsley.<sup>3</sup> The small periodicity might be related to the size of 2- (N, N-dimethyl) amide -1- ethyl group. The distance between two methyl groups attached with nitrogen atom in the functional group is about 0.5 nm measured from the optimized structure of 2- (N, N-dimethyl) amide -1- ethyl group, while the distance between two methyl groups in the malonate groups is about 1 nm. It suggests that the steric hindrance decreases with the size of functional group decreasing. The small steric hindrance might be helpful to form a small periodicity of functional groups.

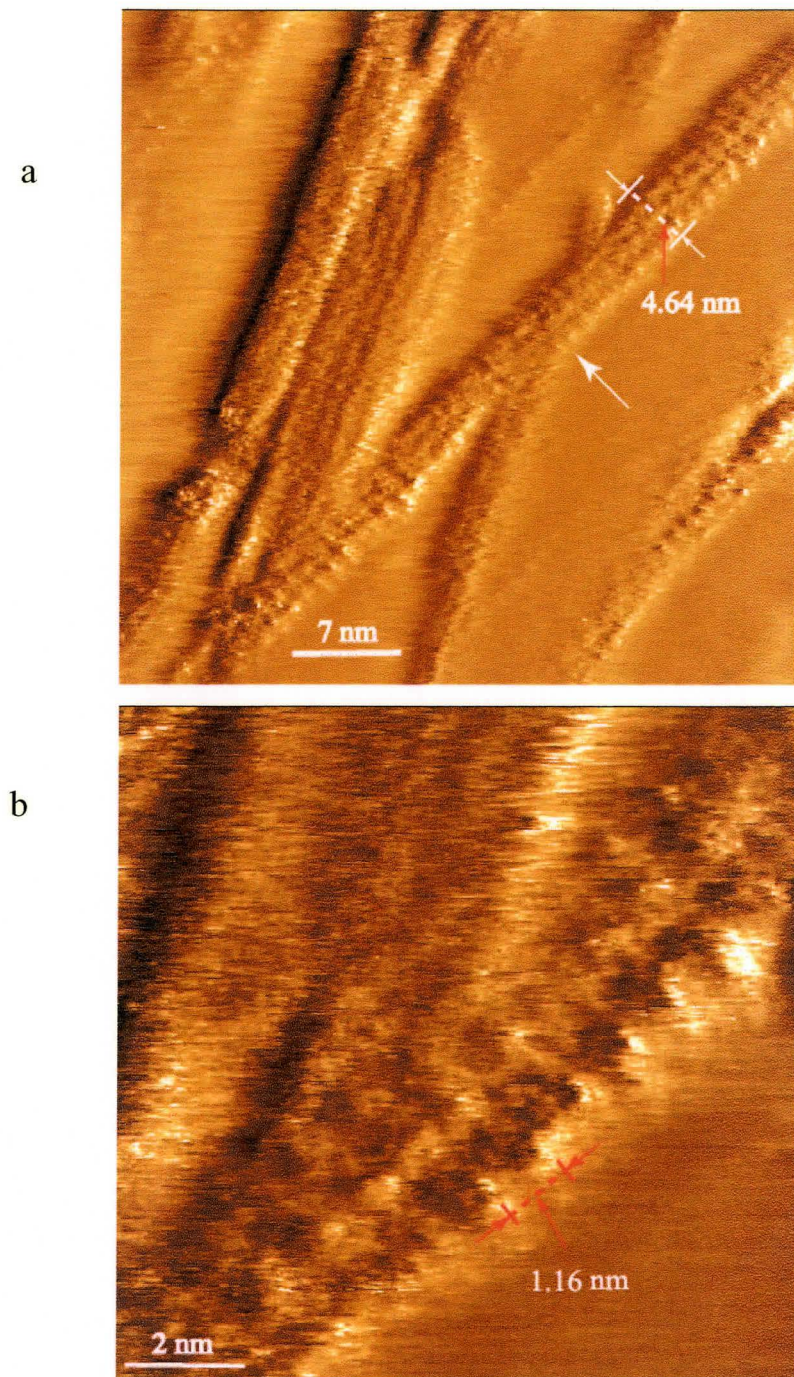


Figure 5-5 The functionalized SWCNTs by isopentyl radicals

a, Scan size: 43.6 nm  $\times$  43.6 nm.  $V_B = 124.8$  mV.  $I_T = 1.5$  nA. Scan rate: 5.79 Hz.

b, Scan size: 11.4 nm  $\times$  11.4 nm.  $V_B = 124.8$  mV.  $I_T = 1.5$  nA. Scan rate: 19.53 Hz

### 5.3.3 Change of electronic structure of SWCNTs after functionalization

In the referer ces, it was said that after functionalization, the electronic structure of nanotubes was changed. Through observing the functionalized SWCNTs via the Bingel reaction, the STM images with atomic resolution showed the consistency with the predictions.

Figure 5-6 shows the STM images with atomic resolution obtained from the functionalized SWCNTs via the Bingel reaction. The honeycomb lattice of the graphite surface was observed in Figure 5-6a, similar to the honeycomb lattice of the graphite surface with STM reported by Tascon's group<sup>13</sup> and with AFM reported by Castle's group.<sup>14</sup> The distance between hollow sites in Figure 5-6a is about 0.24 nm, a little smaller than the real distance 0.246 nm published in the paper,<sup>15</sup> illustrated in Fig. 5c. The white lattice drawn in Figure 5-6a is parallel to the directions of the graphite lattice. Although the STM image shows a little thermal drift in some area, the directions of the graphite lattice on both sides of the structure marked by the letter A are the same as each other, which indicates that the structure marked by the letter A is not grain boundary but a nanotube as explained in Chapter 2. Two bright dots, each of which is surrounded by one dashed elliptical ring, are aligned on this nanotube. The distance between the dots is about 5.86 nm. Through the measurement on another nanotube in Figure 5-6a, the

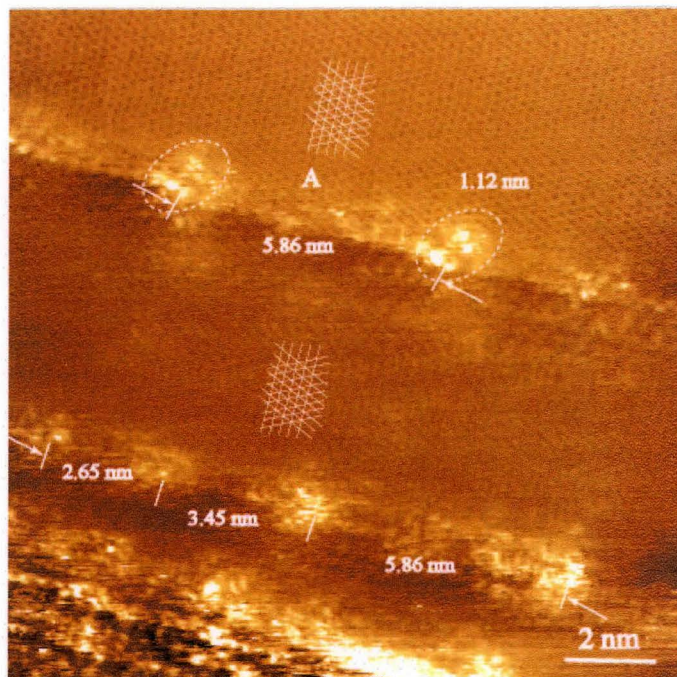


Figure 5-6a The SWCNTs functionalized via the Bingel reaction scan size:  
 $15 \text{ nm} \times 15 \text{ nm}$ .  $V_B = 20.14 \text{ mV}$ .  $I_T = 1 \text{ nA}$ . Scan rate:  $19.53 \text{ Hz}$

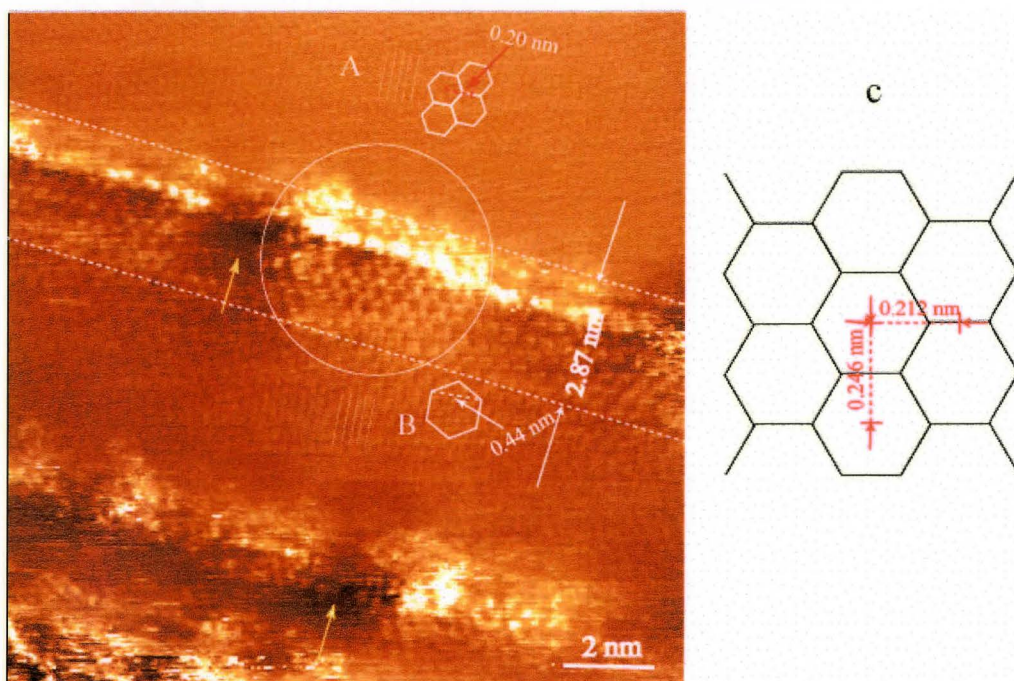


Figure 5-6b, The SWCNTs functionalized via the Bingel reaction scan size:  
 $15 \text{ nm} \times 15 \text{ nm}$ .  $V_B = 20.14 \text{ mV}$ .  $I_T = 1 \text{ nA}$ . Scan rate:  $19.53 \text{ Hz}$ .  
 c, The scheme of the graphite surface.

distance between the neighboring bright dots is various, such as 2.65 nm, 3.45 nm and 5.86 nm, respectively. In the above section, we mentioned that the size of the functional group from the optimized structure with Hyperchem 6.0 is about 1.0 nm. The large functional group tends to increase the steric hindrance, which indicates that the large distance more than 2.5 nm between neighboring groups should be related to the size of the groups. With the size of functional group increasing, the smallest distance between neighboring groups increases. Through careful observation of the bright dots surrounded by a dashed elliptical ring, each of them is composed of two small parts. In addition, the size of each bright dot is about 1.12 nm, similar to the distance between two methyls in one malonate group. Comparing the STM images showing the functionalized SWCNTs one another, we know that the functionalized segments of SWCNTs appear bright. As a result, the bright dots surrounded by a dashed elliptical ring should be malonate groups.

The STM image as shown in Figure 5-6b was obtained from one segment of the nanotube. Both of STM images shown in Figure 5-6a and b are captured from the different segments of the same nanotube. In Figure 5-6b, although the lattice of the graphite surface is not apparent with a little thermal drift, one direction of the graphite surface is determined. The parallel lines are drawn along one direction of the graphite lattice. Comparing the directions of the graphite lattice in **A** area with in **B** area, the

lattice directions on both sides of the structure between two dashed lines are the same as each other, which indicates that the observed structure is not a grain boundary of graphite but a real nanotube.<sup>16</sup> From the STM image in Figure 5-6b, we found that the electronic structure of nanotube sidewall is much different from the graphite lattice. Due to the obscure borders between this nanotube and the graphite surface, two dashed lines were drawn at the borders between the electronic structure of the functionalized nanotube sidewall and the graphite lattice. The distance between two dashed lines is approximately equal to the diameter of this nanotube about 2.87 nm. The honeycomb structure of the graphite surface is not distinct maybe due to the state change of the STM tip during the process to capture this image. Through measuring the distance between two hollow site rows along the directions of the parallel lines in the area **A**, it is found that the distance is about 0.20 nm as shown by the red dashed line in the drawn structure of the graphite substrate, a little smaller than the corresponding distance 0.212 nm reported in the paper.<sup>15</sup> Some hexagonal superlattice structures appear on the functionalized nanotube sidewall. They are surrounded by one white ring as shown in Figure 5-6b. Their size is about 0.44 nm as expressed by the white dashed line in the drawn hexagon of the area **B**, which is about two times of the honeycomb size 0.246 nm of the graphite substrate. In addition, the superlattice structures did not appear in the every area on the sidewall. We

found that they preferred to show up in the area near to the functional groups. The area circled by the large ring appears as the bright band without break, which means that functional groups are covalently bonded on the sidewall in a high density. The superlattice structures did not appear in the area with the small bright dots, the lower degree of functionalization. It can be concluded that the high degree of functionalization on nanotube sidewall would lead to the large change of electronic structure of nanotube sidewall, different from the honeycomb of the unfunctionalized nanotubes. The electronic structure of the functionalized carbon nanotube sidewall shown in Figure 5-6b is very similar to the simulated electronic structure of the fluorinated nanotube reported by Halas group. It can be explained that a  $sp^3$ -hybridized defect alters the original  $sp^2$  bonding of the neighboring C atoms as reported in the paper.<sup>17</sup> The sidewall functionalization disturbed the original  $\pi$ - $\pi^*$  band crossing resulting in a band gap between the conduction and valence bands due to strong tube-molecule interaction, which induced the superlattice on the functionalized nanotube sidewall. We also observed the dark dots on the nanotubes pointed by the yellow arrows, which might be unfunctionalized segments of the carbon nanotube. However, compared with the other unfunctionalized segments, the color is too dark and the dark dots are near to the high functionalized segments of SWCNTs, which indicates that it is possible that the dark dots are the distorted parts of the nanotubes

resulting from functionalization. This speculation is consistent with the calculation of the SWCNT functionalized by  $-\text{COOH}$  group.<sup>18</sup> It is said that the structural distortion on the nanotube is confined to the nearest neighbors of the bonding site and the  $\text{COOH}$  group induces a local distortion along the radical direction on the tube sidewall resulting from the local  $\text{sp}^3$  rehybridization of C-C bonding.<sup>18</sup> In addition, the mechanical strength of CNTs degraded due to the introduction of  $\text{sp}^3$ -hybridized carbon nanotube defects after functionalization.<sup>19</sup> It suggests that the high degree of functionalization on sidewall might lead to the compression of the nanotube to produce kinks or buckles as the shape of the dark dots. After covalent sidewall functionalization, both the electronic structure and the mechanic properties of SWCNTs might be changed depending on the degree of functionalization.

#### 5.3.4 Mixture of electronic structures in the bundles

During the process to observe the functionalized SWCNTs, the large bright bundles of nanotubes are always found on the graphite surface without functional group. Although it is impossible that all of nanotubes are functionalized, some of nanotubes must be functionalized. However, we seldom observed functional groups on the large bundles. In this section, we demonstrated the process to find functional groups in the

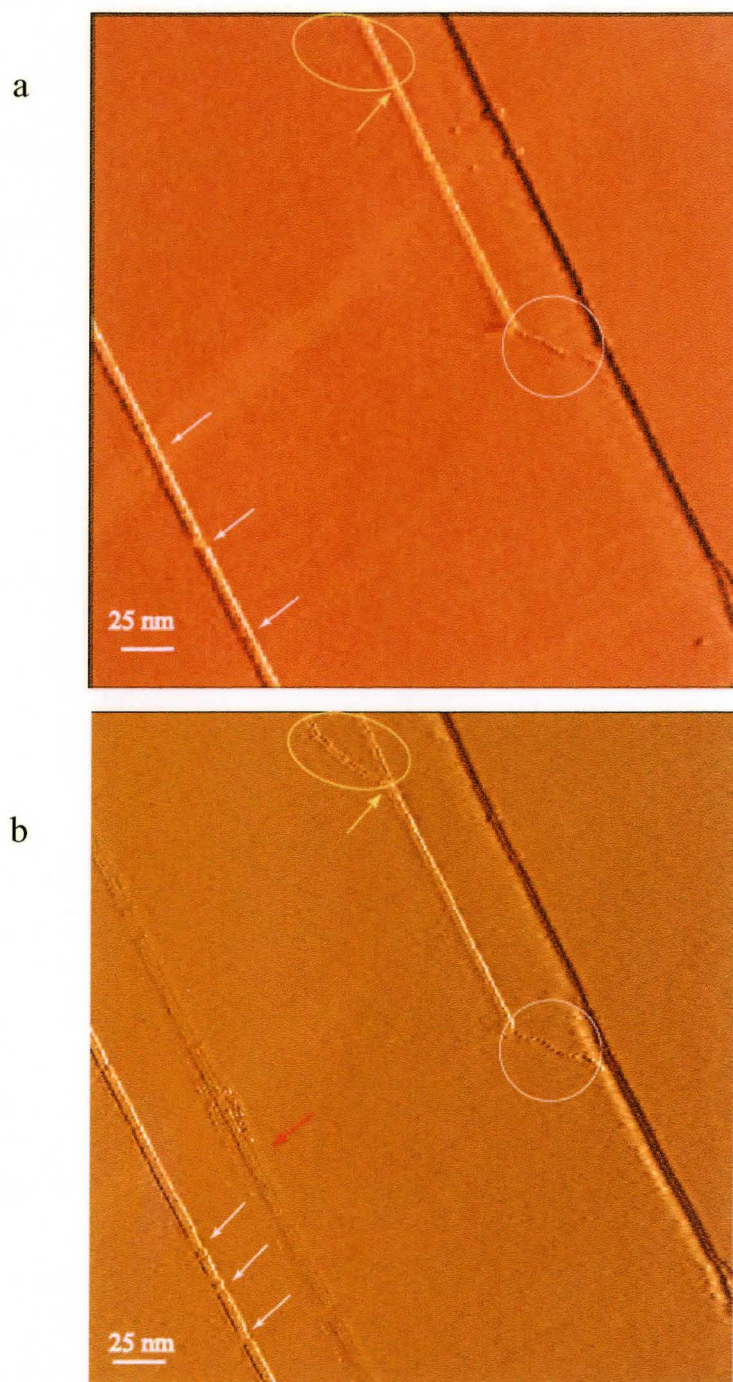


Figure 5-7 (a, b) The process to separate nanotubes from the bundle: scan size:  $322 \text{ nm} \times 322 \text{ nm}$ .  $V_B = 500 \text{ mV}$ .  $I_T = 1 \text{ nA}$ . Scan rate:  $1.93 \text{ Hz}$

large bundle.

Figure 5-7 demonstrates the process to separate nanotubes from the bundle. In Figure 5-7a, two nanotube bundles with similar diameter appeared on the graphite surface. The one at the left corner showed some indentations pointed by white arrows. It suggests that the nanotubes in the bundle are partly functionalized. Another bundle's tail was connected with a small bundle as shown by the white ring. The place pointed by the yellow arrow is the beginning where the large bundle split up into two small bundles in the succeeding image. The area circled by one yellow ellipse only showed one part of the large bundle without any feature. However, after increasing scan rate at one higher value to image the same area for one hour, one interesting thing happened. The nanotube bundle in the place pointed by the yellow arrow began to split up into two similar bundles with the similar diameter to that of the large bundle. It seemed that one bundle was removed from the top of another bundle. Even if the scan rate was reset to the same low value, the two separated bundles can not be incorporated into one large bundle as seen in Figure 5-7b. In addition, each separated bundle exhibited the evidence of functional groups. We can see that each bundle is composed of two nanotubes as shown in the yellow ellipse. The two nanotubes are separated from each other with a certain distance. The color contrast suggests that the functional groups are aligned on each nanotube.

However, we can not decide the existence of the periodicity due to the lack of the image with higher magnification. From the two images Figure 5-7a and b, we can conclude that 1) when the nanotube bundles exactly overlap with each other, it is impossible to observe the functional groups on the nanotubes with STM. It might be due to the mixture of electronic structures of nanotubes in the bundle. Lieber et al. ever mentioned that within a tightly packed nanotube rope, the  $\pi$  and  $\pi^*$  bands of armchair (n, n) SWCNTs are allowed to mix resulting in a pseudogap at the Fermi energy.<sup>12</sup> Our results indicate that functional groups can not be determined on the overlapped nanotube bundles. The interaction between nanotubes will affect the electronic properties of nanotubes resulting in missing the observation of functional groups. 2) To increase the scan rate might make nanotubes separate from each other.

In Figure 5-7b, we also observed that the new nanotube bundle appeared as pointed by a red arrow. It suggests that the tip might move the nanotube bundle from one area to another area. In the area circled by the white round ring, the dark dots are arranged along the small nanotube bundle. We proposed that functionalization changed the electronic properties of nanotube resulting in the presence of the dark dots.

## 5.4 Conclusions

In summary, the correlation extensively exists not only between the bundles but also between the nanotubes in the same bundle. It suggests that one large bundle in solution probably splits up into a few small bundles after it was deposited on the substrate due to the interaction between nanotube and the substrate. After covalent sidewall functionalization, the electronic structure and the mechanical properties of the nanotubes will be affected by functional groups. When the nanotube bundles completely overlap with each other, the functional groups on the nanotubes can not be resolved with STM due to the mixture of the electronic structures of nanotubes. Changing scan rate might make nanotubes separate from each other.

Although functionalization of SWCNTs can decrease the diameter of nanotube bundles, it can not eliminate the aggregation of nanotubes completely. Some small bundles still exist in the solution even under sonication for a few hours.

## References

1. Ying Y, Saini RK, Liang F, Sadana AK, Billups WE. Functionalization of carbon nanotubes by free radicals. *Org. Lett.* 2003;5:1471-1473.
2. Coleman KS, Bailey SR, Fogden S, Green MLH. Functionalization of single-

- walled carbon nanotubes via the Bingel reaction. *J. Am. Chem. Soc.* 2003;125,:8722-8723.
3. Worsley KA, Moonosawmy KR, Kruse P. Long-range periodicity in carbon nanotube sidewall functionalization. *Nano Lett.* 2004;4:1541-1546.
  4. Thess A, Lee R, Nikolaev P, Dai H, Petit P, Rober J, Zu C, Lee YH, Kim SG, Rinzler AG and others. Crystalline ropes of metallic carbon nanotubes. *Science* 1996;273:483-487.
  5. Odom TW, Huang JL, Kim P, Lieber CM. Structure and electronic properties of carbon nanotubes. *J. Phys. Chem. B* 2000;104,:2794-2809.
  6. Rettig C, Bodecker M, Hovel H. Carbon-nanotubes on graphite: alignment of lattice structure. *J. Phys. D: Appl. Phys.* 2003;36:818-822.
  7. Hertel T, Märtel R, Avouris P. Manipulation of individual carbon nanotubes and their interaction with surfaces. *J. Phys. Chem. B* 1998;102:910-915.
  8. Venema LC, Meunier V, Lambin P, Dekker C. Atomic structure of carbon nanotubes from scanning tunneling microscopy. *Phys. Rev. B*, 2000;61:2991-2996.
  9. Ouyang M, Huang JL, Lieber CM. Scanning tunneling microscopy studies of the one-dimensional electronic properties of single-walled carbon nanotubes. *Annu. Rev. Phys. Chem.* 2002;53:201-220.
  10. Maltezopoulos T, Kubetzka A, Morgenstern M, Wiesendanger R, Lemay SG, Dekker C. Direct observation of confined states in metallic single-walled carbon nanotubes. *Appl. Phys. Lett.* 2003;83:1011-1013.
  11. Kelly KF, Chiang IW, Mickelson ET, Hauge RH, Margrave JL, Wang X, Scuseria GE, Radloff C, Halas NJ. Insight into the mechanism of sidewall functionalization of single-walled nanotubes: an STM study. *Chem. Phys. Lett.* 1999;313:445-450.

12. Odom TW, Huang JL, Lieber CM. STM studies of single-walled carbon nanotubes. *J. Phys.: Condens. Matter* 2002;14:R145-167.
13. Paredes JI, Martinez-Alonso A, Tascon JMD. Triangular versus honeycomb structure in atomic resolution STM images of graphite. *Carbon* 2001;39:473-481.
14. Singjai P, Zhdan PA, Castle JE. Observations on the full honeycomb structure of graphite as imaged by atomic force microscopy. *Philos. Mag. A* 2000;80:2445-2456.
15. Toussaint U, Schimmel T, Kupperts J. Computer simulation of the AFM/LFM imaging process: hexagonal versus honeycomb structure on graphite. *Surf. Interface Anal.* 1997;25:620-625.
16. Heckl WM, Binnig G. Domain walls on graphite mimic DNA. *Ultramicroscopy* 1992;42-44:1073-1078.
17. Delaney P, Choi HJ, Ihm J, Louie SG, Cohen ML. Broken symmetry and pseudogaps in ropes of carbon nanotubes. *Nature* 1998;391:466-468.
18. Zhao J, Park H, Han J, Lu JP. Electronic properties of carbon nanotubes with covalent sidewall functionalization. *J. Phys. Chem. B* 2004;108:4227-4230.
19. Garg A, Sinnott SB. Effect of chemical functionalization on the mechanical properties of carbon nanotubes. *Chem. Phys. Lett.* 1998;295:273-278.

## Chapter 6

### Conclusions

#### 6.1 Alignment of copper phthalocyanine (CuPc) compounds on Au(111)

Through using three different methods to prepare the films of CuPc, CuPcSC<sub>5</sub> and CuPcSC<sub>8</sub> on the Au(111) surface, the orientations of those molecules are investigated with scanning tunneling microscopy (STM). It was found that most of the structures of molecules are induced by the STM tip. The interaction between molecules and the gold surface is very weak, even though sulfur atoms are introduced into molecules. Compared to the structure of CuPc without any alkyl chain, CuPcSC<sub>5</sub> and CuPcSC<sub>8</sub> have an improved ability to form ordered structures with the self-assembly method. However, it is difficult to determine the orientation of molecules due to the movement of molecules on the gold surface. The molecules in Langmuir-Blodgett films did not form a regular pattern and the structures of molecules are still affected by the STM tip. CuPcSC<sub>5</sub> and CuPcSC<sub>8</sub> molecules tend to arrange themselves into rod-like columns due to the  $\pi$ - $\pi$  interaction between molecules. Through annealing of the prepared sample, the molecules probably change their structure to form a regular pattern. In addition, we also found that with the length of the substituted alkyl chains decreasing, the molecules formed an ordered pattern more easily.

However, the lack of high-resolution STM images leads to a difficulty in determining the molecular orientation. One way is to increase the interaction between the molecules and the substrate to prevent the mobility of the molecules on the gold surface. Through changing thio-ether groups into thio groups, the chemical bond between the sulfur atom and the gold surface will be formed to assist anchoring of the molecules on the gold surface. Another way is to mix CuPcSC<sub>5</sub> or CuPcSC<sub>8</sub> with other molecules such as stearic acid to increase the interaction between molecules, which makes it possible to obtain a regular pattern.

## 6.2 Sidewall functionalization of SWCNTs

Through the observation of the functionalized SWCNTs formed by the free radical reaction and via the Bingel reaction, the correlation extensively exists between functional groups on the different nanotubes. It suggests that one large bundle in solution probably splits up into a few small bundles after it was deposited on the substrate due to the interaction between nanotube and the substrate. Whether functional groups are bonded on SWCNT with a periodicity or not depends on the electron spatial distribution and the strain within the nanotube caused by the addition of functional groups. After covalent sidewall functionalization, the electronic structure and the mechanical properties

of the nanotubes might be changed by functional groups. The atomic-resolution STM images of the functionalized SWCNTs provide a possibility to investigate the effect of functional groups on electronic structure of nanotubes. Changing scan rate might separate nanotubes from each other.

Although functionalization of SWCNTs can decrease the diameter of nanotube bundles, it can not eliminate the aggregation of nanotubes completely. Some small bundles still exist in the solution even under sonication for a few hours.

The next step would be to find which kind of functional groups can allow nanotubes completely separate from each other in a bundle, how the diameter and the helicity affect the reactivity of nanotubes, how the distribution of functional groups changes the electronic structure of nanotubes. In addition, it is possible to locally observe the process of functionalization of nanotubes at the liquid-solid interface with STM, which will provide the direct evidence to explore the mechanism of functionalization of nanotubes.